Evidence for widespread selection in shaping the genomic landscape during speciation of *Populus*

Jing Wang[1*], Nathaniel R. Street[2], Eung-Jun Park[3], Jianquan Liu[1], Pär K. Ingvarsson[4]

[1] Key Laboratory for Bio-resources and Eco-environment, College of Life Science, Sichuan University, Chengdu, China

[2] Umeå Plant Science Centre, Department of Plant Physiology, Umeå University, 90187 Umeå, Sweden

3 Department of Bioresources, National Institute of Forest Science, Suwon 16631, Republic of Korea

[4] Department of Plant Biology, Uppsala BioCenter, Swedish University of Agricultural Sciences, PO Box 7080, 75007, Uppsala, Sweden

*Correspondence: wangjing2019@scu.edu.cn

Running title: Genomic impact of selection in *Populus*

Abstract

Increasing our understanding of how various evolutionary processes drive the genomic landscape of variation is fundamental to a better understanding of the genomic consequences of speciation. However, the genome-wide patterns of within- and between- species variation have not been fully investigated in most forest tree species despite their global ecological and economic importance. Here, we use whole-genome resequencing data from four *Populus* species spanning the speciation continuum to reconstruct their demographic histories, investigate patterns of diversity and divergence, infer their genealogical relationships and estimate the extent of ancient introgression across the genome. Our results show substantial variation in these patterns along the genomes although this variation is not randomly distributed but is strongly predicted by the local recombination rates and the density of functional elements. This implies that the interaction between recurrent selection and intrinsic genomic features has dramatically sculpted the genomic landscape over long periods of time. In addition, our findings provide evidence that, apart from background selection, recent positive selection and long-term balancing selection are also crucial components in shaping patterns of genome-wide variation during the speciation process.

Keywords: Linked selection, Recombination, Incomplete lineage sorting, Phylogenetic relationship, Ancient introgression, *Populus*

Introduction

Determining the evolutionary forces affecting patterns of genome-wide variation has been a central goal in evolutionary biology over the past several decades (Seehausen et al., 2014). Furthermore, studying variation in levels of differentiation within and between closely related species has the potential to yield important insights into the process of speciation (Ravinet et al., 2017; Wolf & Ellegren, 2017). Studies in a broad range of taxonomic groups have revealed a picture of a highly heterogeneous genomic landscape with peaks and valleys of diversity and differentiation (Han et al., 2017; Nadeau et al., 2012; Stankowski et al., 2019; Turner, Hahn, & Nuzhdin, 2005). Local peaks of elevated divergence are usually referred to as 'speciation islands' and are thought to represent regions that drive the reproductive isolation between incipient species (Abbott et al., 2013; Wu, 2001). Between these islands, gene flow acts to homogenize the reminder of genome and hence acts to limit differentiation (Feder, Egan, & Nosil, 2012; Nosil, Funk, & Ortiz‐Barrientos, 2009). However, a plethora of recent studies highlight that the heterogeneous patterns of differentiation can evolve through processes that are unrelated to speciation *per se* (Burri et al., 2015; Cruickshank & Hahn, 2014). For example, even in the absence of gene flow, natural selection, in the form of either a selective sweep or background selection, can cause reduced genetic diversity not only at the target sites under selection but also at linked neutral sites (Han et al., 2017; Phung, Huber, & Lohmueller, 2016). Such selection could accelerate lineage sorting and will hence inevitably result in increased genetic differentiation between species in these regions (Burri, 2017). Furthermore, the long-term action of linked selection in ancestral as opposed to extant lineages can also affect the amount and distribution of ancestral polymorphisms (Ma et al., 2018; Munch, Nam, Schierup,

& Mailund, 2016; Scally et al., 2012), which can further result in heterogeneous patterns of genealogical relationships among closely related species (Mailund, Munch, & Schierup, 2014; Pease & Hahn, 2013). Despite widespread interest in speciation genomics, there remains little consensus as to how various evolutionary processes have shaped the genomic landscape during the speciation process that eventually gives rise to new species (Ravinet et al., 2017).

Empirical studies suggest that the formation of the genomic landscape of diversity during speciation is highly influenced by the demographic histories of the species, the types of selection acting on different genomic regions and also several other intrinsic genomic features (Burri, 2017; Ellegren & Galtier, 2016). Disentangling the effects of speciation (i.e. species split time, strict isolation or divergence with gene flow) is important for interpreting the patterns of genome-wide variation, because without a clear picture of the demographic history of the descendant species, it is challenging to distinguish whether heterogenous genomic differentiation arose due to genetic drift, local adaptation or introgression (Nadachowska-Brzyska et al., 2013; Ravinet et al., 2018). Furthermore, as the speciation process advances, the evolution of genome-wide patterns of variation can be influenced by different forms of selection (Cutter & Payseur, 2013). Under a background selection model, purifying selection continuously eliminates deleterious mutations, resulting in reduced levels of genetic diversity at linked loci and increased levels of F_{ST} (a relative measure of genetic divergence) (Charlesworth, 2012; Charlesworth, Morgan, & Charlesworth, 1993; Hudson & Kaplan, 1995). Under a selective sweep model, genetic variants linked to beneficial mutations acted upon by positive selection hitchhike along and reach high frequency (Kaplan, Hudson, & Langley, 1989; Smith & Haigh, 1974). Accordingly, even in the absence of gene flow, selection due to, for instance local ecological adaptation, can result in reduced diversity

and increased F_{ST} (Cruickshank & Hahn, 2014). In comparison to purifying and positive selection, long-term balancing selection favors the maintenance of advantageous polymorphisms for many generations, which instead result in genomic regions with elevated genetic diversity and reduced F_{ST} (Charlesworth, 2006; Guerrero & Hahn, 2017). As deleterious mutations are assumed to be much more common compared to beneficial mutations, background selection has been argued to play a major role in the evolution of diversity (Burri, 2017; Lohmueller et al., 2011; Phung et al., 2016). However, many recent simulation studies have shown that background selection alone is far from sufficient for generating the heterogenous genomic landscapes observed in empirical studies of recently diverged species, and other evolutionary processes (such as positive selection) are thus required to explain the observed patterns (Matthey‐Doret & Whitlock 2019; Stankowski et al., 2019).

Regardless of the role of demographic processes and selection, genomic features, such as recombination rate variation and the heterogeneous density of functional sites, are also expected to play key roles in mediating the efficacy and extent of selection and gene flow, as well as how these processes interact as the speciation process proceeds (Flaxman, Wacholder, Feder, & Nosil, 2014; Hurst, Pál, & Lercher, 2004; Nachman & Payseur, 2012). Local rates of recombination interacts with natural selection and are known to have a profound effect on patterns of genomic diversity, incomplete lineage sorting (ILS) and rates of introgression (Begun & Aquadro, 1992; Comeron, Williford, & Kliman, 2008; Cutter & Payseur, 2013). Independent of the recombination rate, the density of functional sites can also influence genome-wide patterns of diversity since functional regions are more likely to experience either stronger effects of positive or purifying selection compared to nonfunctional regions where mutations are assumed to have little effect on fitness (Al-Shahrour et al., 2010;

Nordborg et al., 2005). The long-term diversity-reducing effects of selection in functional regions will reduce locally effective population size (N_e), accelerate lineage sorting and increase genetic divergence between species (Flowers et al., 2011; Hobolth, Dutheil, Hawks, Schierup, & Mailund, 2011). As it becomes increasingly feasible to generate whole genome resequencing data from closely related species, the importance of conserved genomic features in shaping the topography of the genomic landscape of speciation has increasingly been highlighted by several studies in a diverse set of taxa showing highly correlated patterns of differentiation among independently species pairs (Burri, 2017; Delmore et al., 2018; Van Doren et al., 2017; Vijay et al., 2017).

Forest trees provide an excellent system to address the genomic architecture of adaptation and speciation in natural populations because they are mostly undomesticated without much anthropogenic influence, ecologically important across a wide variety of habitats and harbour abundant genetic and phenotypic variation (Neale & Ingvarsson, 2008; Neale & Kremer, 2011). In this study, we focus on four *Populus* species (*Populus tremula*, *P. davidiana*, *P. tremuloides* and *P. trichocarpa*) that span the speciation continuum. All four species are all deciduous, obligated outcrossing tree species that have wide geographical distributions throughout the Northern Hemisphere (Figure 1A). Among them, *P. tremula* (European aspen), *P. davidiana* (Chinese aspen) and *P. tremuloides* (American aspen) are sibling aspen species belonging to the same section of the genus *Populus* (section *Populus*) (Eckenwalder, 1996; Hamzeh & Dayanandan, 2004). Earlier phylogenetic studies have revealed that *P. tremuloides* diverged from the other two species following the break-up of the Bering Land bridge, whereas the uplift of the Qinghai-Tibetan Plateau and the associated climate oscillations may have driven the divergence between *P. tremula* and *P. davidiana* (Du et al., 2015). In addition, these aspen species can readily hybridize and their artificial hybrids show

heterosis for many growth and wood characteristics (Hart, De Araujo, Thomas, & Mansfield, 2013), suggesting that the speciation process has not gone to completion among the three aspen species. In comparison, *P. trichocarpa* belongs to a different section of the genus *Populus* (section *Tacamahaca*), and it is reproductively isolated from all aspen species (Jansson & Douglas, 2007). Facilitated by the availability of a high-quality reference genome of *P. trichocapra* (Tuskan et al., 2006), the four *Populus* species represent a promising model system to investigate how various evolutionary forces have shaped the evolution of the genomic landscape of differentiation across the speciation continuum in forest trees.

We use whole-genome re-sequencing in the four *Populus* species to (i) determine their speciation history and characterize whether there is historical gene flow between the now-allopatric species; (ii) examine the fine-scale genomic landscapes of diversity and divergence across species at different stages of divergence; (iii) quantify the extent of genome-wide genealogical discordance and ancient hybridization among the three closely related aspen species; (iv) identify the signatures of positive selection and long-term balancing selection along the genome, and uncover how they impact levels of variation during speciation. Overall, our main aim is to disentangle and understand how the multitude of evolutionary processes have shaped the genomic architecture during speciation.

2. Materials and Methods

2.1 Sample collection, whole-genome resequencing and genotype calling

We used whole genome resequencing data from eight individuals each of *Populus tremula*, *P. tremuloides* and *P. trichocarpa*, as described in Wang et al. (2016a), and

147 additional eight individuals of *P. davidiana* that are first reported in this study (Table
148 S1). The sampling was from a single geographic region for each species (Figure 1A).
149 Briefly, sequencing of all samples was carried out on the Illumina HiSeq 2000 platform.
150 Prior to read mapping, we used Trimmomatic (Lohse et al., 2012) to remove adapter
151 sequences and to trim low quality bases from the start or the end of reads (base quality≤
152 20). If the processed reads were shorter than 36 bases after trimming, the entire reads
153 were discarded. After quality control, we mapped the remaining reads from each
154 individual to the *P. trichocarpa* reference genome (v3.0) (Tuskan et al., 2006) using
155 BWA-MEM algorithm with default parameters, as implemented in bwa-0.7.10 (Li,
156 2013).

157 To minimize the influence of mapping bias, several further filtering steps were
158 employed before genotype calling. First, we used RealignerTargetCreator and
159 IndelRealigner in GATK v3.8.0 (DePristo et al., 2011) to correct for the mis-alignment
160 of bases in regions around insertions and/or deletions (indels). Second, to account for
161 the artifacts due to PCR duplication introduced during library construction, we used the
162 MarkDuplicates method from Picard packages (http://broadinstitute.github.is/picard/) to
163 only retain the read or read-pair with the highest summed base quality among those with
164 identical external coordinates and same insert lengths. Additionally, we further
165 discarded site types that likely cause mapping bias based on three criteria: (1) those with
166 extreme read coverage (less then 4× or higher than twice of the mean coverage); (2)
167 covered by more than two reads of mapping score equaling zero per individual; (3)
168 overlapping known repetitive elements as identified by RepeatMasker (Tarailo‐
169 Graovac & Chen, 2009). Finally, sites that passed all these filtering criteria were used in
170 downstream analyses. This left a total of 168,950,389 sites for further analysis (42.8%
171 of collinear genomic sequences of the *P. trichocarpa* genome assembly).

After filtering, we implemented two complementary approaches for genotype calling. First, to account for the bias inherent in genotype calling approach from next generation sequencing (NGS) data (Nielsen, Korneliussen, Albrechtsen, Li, & Wang, 2012), the population genetic estimates that relied on site frequency spectrum (SFS) were calculated using ANGSD v0.917 (Korneliussen, Albrechtsen, & Nielsen, 2014). Second, for the analyses that require accurate single nucleotide polymorphism (SNP) calls, genotype calling in each individual was performed using HaplotypeCaller of the GATK v3.8.0, and GenotypeGVCFs was then used to merge multi-sample records from the four species together for re-genotyping and re-annotation of the newly merged VCF (DePristo et al., 2011). To minimize genotype calling bias and to retain high-quality SNPs, we further performed several filtering steps: (1) SNPs that overlapped with sites not passing all previous filtering criteria were removed; (2) only bi-allelic SNPs with a distance of at least 5 bp away from any indels were retained; (3) genotypes with read depth (DP) < 5 and/or with genotype quality score (GQ) < 10 were treated as missing, and we then removed all SNPs with a genotype missing rate > 10%. After all these steps of filtering, a total of 8,568,990 SNPs were retained across the four *Populus* species. For the analyses that required imputed and phased dataset, BEAGLE v4.1 (Browning & Browning, 2009) was used to infer haplotypes of individuals within each species.

2.2 Phylogenetic relationships and population structure analysis

Chloroplast phylogeny

To infer the phylogenetic relationship of the four *Populus* species based on chloroplast data, we first mapped the filtered reads from our resequencing data against the *P. trichocarpa* chloroplast genome using bwa-aln 0.7.10 (Li & Durbin, 2009). Then, UnifiedGenotyper in GATK v3.8.0 was used to call SNPs at all sites (--output_mode

EMIT_ALL_SITES). Since chloroplasts are haploid and SNPs are thus expected to be homozygous, the haploid option (-ploidy 1) in UnifiedGenotyper was used. After treating sites with GQ < 30 as missing data, only bi-allelic SNPs with quality by depth (QD) ≥ 10 and with a missing rate ≤ 20% were retained. Finally, a consensus tree was constructed based on 1,292 chloroplast SNPs using maximum likelihood method implemented in SNPhylo (Lee, Guo, Wang, Kim, & Paterson, 2014).

Principle component analysis (PCA)

To account for the uncertainty in genotype calls, PCA was performed using ANGSD v0.917 and ngsTools v1.0.1 (Fumagalli, Vieira, Linderoth, & Nielsen, 2014). We first used the SAMTools model (Li et al., 2009) in ANGSD to estimate genotype likelihoods from BAM files using only reads with a minimal base quality score of 20 and a minimal mapping quality score of 30 across all individuals. ngsTools was then used to compute the expected covariance matrix across pairs of individuals for the four species based on the genotype posterior probabilities across all filtered sites. Eigenvectors and eigenvalues were generated with the R function eigen from the covariance matrix, and the significance level was determined using the Tracy-Widom test as implemented in EIGENSOFT version 6.1.4 (Patterson, Price, & Reich, 2006).

Identity-by-descent (IBD) blocks analysis

To determine the extent to which individuals across the four species shared DNA segments, the identity-by-descent block analysis was performed for the four species using BEAGLE v4.1 (Browning & Browning, 2013) with the following parameters: window=100,000; overlap=10,000; ibdtrim=100; ibdlod=5.

2.3 Demographic history reconstruction

MSMC

We used Multiple Sequentially Markovian Coalescent approach (MSMC v2) (Schiffels & Durbin, 2014) to infer patterns of historical patterns of effective population sizes changes through time for all four *Populus* species. Only sites passing all above filtering criteria were included in analyses. Because different number of individuals and haplotypes provides different resolution for recent and distant population histories, we applied MSMC to phased whole-genome sequences from one (two haplotypes, which can infer more distant size changes), two (four haplotypes, which infer size changes at intermediate time scales) and four (eight haplotypes, which infer the most recent size changes) individuals for each species, respectively. We did not include more haplotypes due to the computational cost of using larger haplotype sets. In total, we have 8, 28 and 70 different individual configurations for two-, four-, and eight- haplotype analyses in each species. We ran MSMC on all individual configurations and estimated medians and standard deviations of effective population sizes changes across time. To convert the coalescent scaled time to absolute time in years, we used a mutation rate of 2×10^{-9} per site per year (Koch, Haubold, & Mitchell-Olds, 2000) and a generation time of 15 years.

Fastsimcoal2

Given the long divergence time and the low number of polymorphic sites shared between aspens and *P. trichocarpa* (Wang, Street, Scofield, & Ingvarsson, 2016a), we used a coalescent simulation-based method implemented in *fastsimcoal2.6* (Excoffier, Dupanloup, Huerta-Sánchez, Sousa, & Foll, 2013) to only infer the demographic and speciation histories only for the three aspen species. For all possible pairs of the three

247 species, the two-dimensional joint SFS (2D-SFS) was constructed from the posterior
248 probabilities of sample allele frequencies using ANGSD v0.917 (Figure S1). A total of
249 twenty-nine models were evaluated and all models began with the split of an ancestral
250 population into the Eurasia and the North America lineage (*P. tremuloides*) followed by
251 the split of the Eurasian lineage into *P. tremula* and *P. davidiana*. The models differed
252 in terms of (1) whether post-divergence gene flow was present or not, (2) time, level
253 and pattern of gene flow between the three aspen species, and (3) the occurrence and
254 pattern of population expansion in *P. tremuloides* given a genome-wide excess of rare
255 frequency alleles that we observed in this species in our previous study (Wang et al.,
256 2016a) and also in this study (Figure S2). Alternative demographic models were fitted
257 to the joint SFS data. The global maximum likelihood estimates for all demographic
258 parameters under each model were obtained from 50 independent runs, with 100,000
259 coalescent simulations per likelihood estimates (-n 100000, -N 100000) and 40 cycles of
260 the likelihood maximization algorithm. The models were compared based on the
261 maximum value of likelihood over the 50 independent runs using the Akaike's weight
262 calculated following Excoffier et al. (2013). The model with the maximum Akaike's
263 weight value was chosen as the optimal one. Confidence intervals were generated by
264 performing parametric bootstrapping with 100 bootstrap replicates, and with 50
265 independent runs in each bootstrap. As for MSMC, we assumed a mutation rate of
266 2×10^{-9} per site per year and a generation time of 15 years (Koch et al., 2000) when
267 converting estimates to units of years and individuals.
268
269 ***2.4 Intra- and inter- species summary statistics***
270 *Intra-species genomic diversity*

For each species, based on the SAMTools genotype likelihood model (Li et al., 2009), we used ANGSD v0.917 (Korneliussen et al., 2014) to estimate allele frequency likelihoods, obtain a maximum likelihood estimate of the folded site frequency spectrum and used this to calculate nucleotide diversity (π) in non-overlapping sliding windows of 10 Kbp and 100 Kbp across the entire genome. Only sites with a minimum mapping quality of 30 and minimum base quality of 20 were used in the estimation. Windows were discarded if there were less than 10 % sites left after all of the filtering steps described above. Since our previous study showed that linkage disequilibrium (LD) decays within 10 Kbp in different species of *Populus* (Wang et al., 2016a), in the following we focused more on estimates derived from 10 Kbp windows.

Inter-species genomic divergence

For each species pair, we estimated two divergence metrics across the 10 Kbp and 100 Kbp non-overlapping windows: genetic differentiation (F_{ST}) and sequence divergence (d_{xy}). Without relying on SNP or genotype calling (Fumagalli et al., 2013), we first used ANGSD to calculate posterior probabilities of sample allele frequency for each species. Then, the program ngsFST from the ngsTools package was used to estimate F_{ST} between species using a method-of-moments estimator, and the program ngsStat was used to calculate d_{xy} between species at each site. Finally, we averaged these divergence values across all sites within each window.

Population-scaled recombination rate

For each species we used LDhelmet v1.9 (Chan, Jenkins, & Song, 2012), a coalescent-based, reversible-jump Markov chain Monte Carlo (rjMCM) simulation method, to estimate the population-scaled recombination rate, ρ. First, VCFtools

296 (Danecek et al., 2011) and custom shell script were used to tailor the phased genotype
297 data of each chromosome to the necessary input sequence file (fasta format). Then, we
298 used 'find_confs' in LDhelmet to concatenate all the input sequences files and generate
299 a haplotype configuration file per species. Thereafter, 'table_gen' was used to compute
300 the likelihood lookup table for each species, where we assume the approximate
301 genome-wide neutral diversity (θ) of 0.01 for the three aspen species and of 0.005 for *P.*
302 *trichocarpa* (Wang et al., 2016a), and the grid of ρ values was specified as –r 0.0 0.1
303 10.0 1.0 100.0 for all species. In addition, the optional 'pade' component of LDhelmet
304 was included in the analysis, which computes the Padé coefficients (-x 11) from the
305 haplotype configuration file. Finally, we ran LDhelmet with window size of 50 SNPs
306 and block penalty of 50 for a total of 1,000,000 iterations, discarding the first 100,000
307 as burn-in. We then calculated weighted average of the estimated ρ in 10 Kbp and 100
308 Kbp windows, respectively. Windows with less than 50 SNPs (for 10 Kbp windows)
309 and 200 SNPs (for 100 Kbp windows) left from previous filtering steps were discarded.
310

311 ***2.5 Window-based phylogenomic analysis***

312 *Topology weighting*

313 As expected for a clade with rapid radiation, genealogies may vary widely across
314 different genomic regions (Lamichhaney et al., 2015). Given that *P. trichocarpa* is
315 distantly related from the other three aspen species (Hamzeh & Dayanandan, 2004), we
316 used Twisst, a topology weighting method by iterative sampling of subtrees (Martin &
317 Van Belleghem, 2017), to assess and quantify the phylogenetic discordance among the
318 three aspen species along the genome. The genealogical relationships of these species
319 can be defined by three possible topologies: [(*P. tremula*, *P. davidiana*), *P.*
320 *tremuloides*], [(*P. tremula*, *P. tremuloides*), *P. davidiana*], [(*P. davidiana*, *P.*

tremuloides), *P. tremula*]. Using *P. trichocarpa* as the outgroup species, local phylogenetic subtrees was inferred in RAxML v8.2.4 (Stamatakis, 2014) with the GTRCATI model over non-overlapping 10 Kbp and 100 Kbp windows. Topology weightings for each window were then computed through determining the number of unique subtrees that match each of the three possible topologies by iteratively sampling a single haplotype from each species (Martin & Van Belleghem, 2017). Windows were discarded in topology weighting estimation if there were < 50 SNPs and < 200 SNPs left from previous filtering steps for 10 Kbp and 100 Kbp windows, respectively.

Inference of incomplete lineage sorting

Because the speciation events that resulted in aspen species were close in time (see Results), we expect the lineage sorting process relating these species to be incomplete. Given the three aspen species and the outgroup poplar species (*P. trichocarpa*) with the relationship as (((*P. tremula*, *P. davidiana*), *P. tremuloides*), *P. trichocarpa*), we labeled alleles in *P. tremula*, *P. davidiana* and *P. tremuloies* as A (ancestral allele) if they match the reference allele of *P. trichocarpa* genome, and B (derived allele) otherwise. We then considered segregating sites with (((*P. tremula*, *P.davidiana*), *P. tremuloides*), *P. trichocarpa*) patterns as AABAs, ABAAs, BAAAs, ABBAs, BABAs and BBAAs. The two SNP patterns ABBAs and BABAs can result from incomplete lineage sorting if we assume no gene flow occurred among species (Durand, Patterson, Reich, & Slatkin, 2011; Green et al., 2010). We calculated the level of incomplete lineage sorting (ILS) at site *i* in the genome as:

$$ILS=(C_{ABBA(i)}+C_{BABA(i)})/h \quad (1)$$

$$\text{where } h=(C_{BAAA(i)}+C_{ABAA(i)}+C_{AABA(i)}+2(C_{BBAA(i)}+C_{BABA(i)}+C_{ABBA(i)})/3 \quad (2)$$

Because population samples were used for all species, at each site we used the frequency of the derived allele in each species to effectively weight each segregating site according to its fit to the six segregation patterns for the three aspen species (Durand et al., 2011), with

$$C_{BAAA(i)}=\hat{p}_{i1}(1-\hat{p}_{i2})(1-\hat{p}_{i3})(1-\hat{p}_{i4}) \quad (3)$$

$$C_{ABAA(i)}=(1-\hat{p}_{i1})\hat{p}_{i2}(1-\hat{p}_{i3})(1-\hat{p}_{i4}) \quad (4)$$

$$C_{AABA(i)}=(1-\hat{p}_{i1})(1-\hat{p}_{i2})\hat{p}_{i3}(1-\hat{p}_{i4}) \quad (5)$$

$$C_{BBAA(i)}=\hat{p}_{i1}\hat{p}_{i2}(1-\hat{p}_{i3})(1-\hat{p}_{i4}) \quad (6)$$

$$C_{BABA(i)}=\hat{p}_{i1}(1-\hat{p}_{i2})\hat{p}_{i3}(1-\hat{p}_{i4}) \quad (7)$$

$$C_{ABBA(i)}=(1-\hat{p}_{i1})\hat{p}_{i2}\hat{p}_{i3}(1-\hat{p}_{i4}) \quad (8)$$

where $\hat{p}_{ij}$ is the frequency of the derived allele at site i in species j.

The calculation of ILS presents the counts of incomplete lineage sorting pattern ($C_{ABBA(i)}$ and $C_{BABA(i)}$) normalized by the total count of segregating sites (h), which is a proxy of the species tree topology height (Scally et al., 2012). We then summarized the proportion of ILS over non-overlapping 10 Kbp and 100 Kbp windows or in bins with varying distances from the nearest exon.

2.6 Analyses of introgression

We first tested for introgression between the three aspen species using the *D*-statistic, also known as the ABBA-BABA tests. These tests evaluate the imbalance frequency of site patterns (Durand et al., 2011; Green et al., 2010). Using *P. trichocarpa* as the

outgroup, we expect equal counts of the two site patterns (ABBA and BABA) when incomplete lineage sorting causes the site pattern discordance. If discordance is caused by introgression, one of the site patterns is expected to be more prevalent than the other. We applied two approaches to perform the *D*-statistic test. First, we used –doAbbababa2 implemented in ANGSD v0.917 (Korneliussen et al., 2014) to directly count ABBA and BABA sites and calculate the *D* statistic without calling genotypes in non-overlapping 10 Kbp and 100 Kbp windows for the whole genome. Then, jackknife bootstrapping was conducted to estimate significance at the chromosome and whole-genome level. Second, based on allele frequencies at each SNP called by GATK, we calculated the *D* statistic in 10 Kbp and 100 Kbp non-overlapping windows across the genome with the python script *ABBABABAwindows.py* (https://github.com/simonhmartin/genomics_general) (Martin, Davey, & Jiggins, 2014). Following the detection of introgression among individuals at the genome level, we used a modified *f*-statistic (f_d) (Martin et al., 2014) to estimate the proportion of introgressed sites at the population level using *ABBABABAwindows.py* (https://github.com/simonhmartin/genomics_general) on non-overlapping 10 Kbp and 100 Kbp windows across the genome.

2.7 ***Genome-wide scan for regions under positive and balancing selection in aspens***

To specifically test for the impact of positive and balancing selection on the genomic landscape during speciation of aspens, we first used a composite likelihood ratio (CLR) statistic implemented in SweepFinder2 (DeGiorgio, Huber, Hubisz, Hellmann, & Nielsen, 2016) to detect regions subject to recent positive selection or selective sweeps in each of the three aspen species. The ancestral allelic state was defined by assuming that the alleles that were the same as those found in the *P. trichocarpa* reference

396 genome was the ancestral alleles. By contrasting the likelihood of the null hypothesis,
397 based on the unfolded site frequency spectrum (SFS) calculated across the genome
398 using –f option, with the likelihood of a model where the SFS has been altered by a
399 recent positive selection event, the CLR statistics was calculated in non-overlapping
400 windows of 10 Kbp. Within each species, windows with CLR values higher than the
401 99^{th} percentile of its distribution were identified as candidate region under selection.

402 Moreover, we identified regions under long-term balancing selection by estimating
403 the summary statistics, β (beta score), which detects the clusters of variants with an
404 excess number of intermediate frequency polymorphisms (Siewert & Voight, 2017).
405 Given that the signals of long-term balancing selection usually is localized to a narrow
406 genomic region (Gao, Przeworski, & Sella, 2015), we used 1 Kbp windows to calculate
407 β values for each core SNPs in the three aspen species. We used the unfolded version of
408 β, with the ancestral and derived allelic states inferred based on comparisons with the
409 outgroup species *P. trichocarpa*. To prevent false positives, we filtered out SNPs with a
410 folded frequency lower than 20%, and defined the SNPs with extreme β scores in the
411 top 1% as significant. Furthermore, only SNPs that are significant in all three species
412 were considered as putative targets of long-term balancing selection. Finally, we binned
413 significant SNPs into 10 Kbp windows for downstream comparisons.

414 Lastly, to assess the effects of positive and balancing selection on the genomic
415 architecture of speciation, we compared outlier windows that were identified as being
416 under positive or balancing selection with the remaining genomic regions using a
417 variety of population genetic statistics, including genetic diversity, divergence, lineage
418 sorting and introgression within and between the three closely related aspen species.
419 Differences between outlier windows and the genome-wide averages for all these
420 statistics were tested using Wilcoxon ranked-sum tests. To further examine whether any

functional classes of genes were over-represented in these candidate regions, we performed gene ontology (GO) analyses using the R package topGO 2.36.0 (Alexa & Rahnenführer 2009). Fisher's exact test was used to calculate the statistical significance of enrichment, and GO terms with *P*-value lower than 0.01 were considered to be significantly enriched.

3. Results

3.1 Phylogenetic relationships, population structure and demographic history

The genome alignment resulted in an average depth of 24.6× across all individuals after quality control (Table S1). The PCA results revealed a clear distinction among the four *Populus* species (Figure S4). Based on the Tracy-Widom test, only the first three components were significant (Table S2). The first principal component (PC1; variance explained=28.79%) separated *P. trichocarpa* from the three aspen species, while the second component (PC2; variance explained=7.52%) separated *P. tremuloides* from *P. tremula* and *P. davidiana*. Finally, the third component (PC3, variance explained=5.33%) separated *P. tremula* and *P. davidiana*. The clustering and genetic relationships of the four species were also confirmed by the phylogenetic tree constructed based on the entire chloroplast genomes (Figure 1B). Moreover, we measured the number and length of shared IBD haplotypes within and between species (Figure S5, S6; Table S3, S4). Compared to between-species comparisons, we found much more extensively shared IBD haplotypes for within-species comparisons (Figure S5), although haplotypes shared within *P. tremuloides* were shorter than the other three species (Figure S6A; Table S4). This is likely owing to the higher recombination rate and more rapid decay of linkage disequilibrium (LD) in *P. tremuloides* than other species (Wang et al., 2016a). For the between-species comparisons, we did no observe

any haplotype sharing between the three aspen species and *P. trichocarpa*, confirming the distant relationship between aspens and poplars in the genus *Populus* (Figure S5, Table S3). Within aspens, *P. tremula* and *P. davidiana* shared more and longer haplotypes than either of them shared with *P. tremuloides* (Figure S5, S6B; Table S3, S4), which also supports a closer relationship between these two species, as identified in the chloroplast phylogeny.

To investigate the demographic and speciation histories of the four *Populus* species, we first used MSMC to examine historical fluctuations in the effective population size (N_e) for each species. The results showed that all species experienced a period of population decline during the early Pleistocene cooling (2.5-0.9 million years ago, Mya) (Figure 1C). Compared with the three aspen species, *P. trichocarpa* experienced a more dramatic population decline during this period (Figure 1C, Figure S7), which likely explain the much lower genetic diversity observed in this species relative to others (Table S5). The two North American species, *P. tremuloides* and *P. trichocarpa*, experienced a population expansion from the start of the last ice age (110 thousand years ago, Kya) until the last glacial maximum (LGM, 23-18 Kya) whereas the European species *P. tremula* remained relatively stable. On the other hand, the eastern Asian species, *P. davidiana*, showed pattern of population decline during the entire period (Figure 1C, Figure S7). Our results therefore revealed that before the LGM, forest trees distributed in different continents experienced asynchronous demographic responses to Pleistocene climate changes (Bai et al., 2018). During and following the LGM, all four species experienced a population decline followed by a subsequent rapid population expansion (Figure 1C).

Because of the distant phylogenetic relationship and low levels of shared polymorphism between *P. trichocarpa* and the three aspen species (Wang et al., 2016a),

we therefore explicitly focused on inferring the demographic parameters of the speciation history for the three aspens. After evaluating a total of twenty-nine models (Figure S8), the best-supported model (Figure S8; Table S6) suggests that the Eurasian lineage (the common ancestor of *P. tremula* and *P. davidiana*) split from the North American lineage (*P. tremuloides*) at ~ 2.4 Mya (bootstrap range [BP]: 2.1-3.2 Mya), which is in accordance with our earlier estimates on the divergence time between *P. tremula* and *P. tremuloides* (Wang, Street, Scofield, & Ingvarsson, 2016b). The European lineage (*P. tremula*) and the East-Asian lineage (*P. davidiana*) diverged ~1.7 Mya (BP: 1.5-2.1 Mya) (Figure 1D, Table S7). Our results detected low levels of ancient gene flow between *P. tremula* and *P. davidiana*, and between *P. tremula* and *P. tremuloides* following speciation until around 847 Kya (BP: 539Kya-1.0 Mya) (Figure 1D). After this period the species have remained isolated which is also reflected by their current disjunct geographic distributions (Figure 1A). Compared to the Eurasian lineage of aspens, *P. tremuloides* has experienced a notable population expansion in the recent past (~772 Kya, BP: 440-887 Kya), which is consistent with its genome-wide excess of rare alleles (Figure S2).

3.2 General patterns of genome-wide diversity and differentiation

We further characterized genome-wide patterns of nucleotide diversity (π), population recombination rate (ρ) and divergence (F_{ST} and d_{xy}) for the four *Populus* species (Figure 2A; Table S5, Table S8-S10). At the species level, π varied markedly between species, ranging from 0.0063 in *P. trichocarpa* to 0.0148 in *P. tremuloides*, but the average genomic diversity was very similar across the three aspen species (Table S5). In contrast to the patterns observed for π, the population-scaled recombination rate, ρ, was much higher in *P. tremuloides* (0.0273 bp^{-1}) than in the other three species

496 (0.0096 bp^{-1}-0.0139 bp^{-1}) (Table S8). Variation in genetic divergence (F_{ST} and d_{xy})
497 among the six species pairs reveals the continuous nature of differentiation along the
498 speciation continuum, with *P. tremula* and *P. davidiana* showing the lowest levels of
499 divergence and with the highest divergence observed between aspens and *P.*
500 *trichocarpa* (Figure 2A, Table S9, S10).

501 At the genome level, patterns of genetic diversity and divergence show high levels
502 of parallelism in all pairwise comparisons. The genome-wide profiles of π (average
503 Spearman's ρ =0.71) and ρ (average Spearman's ρ =0.18) were positively correlated in
504 all possible species pairs (Figure 2B, Table S11). We found little evidence for an
505 association between either π or ρ and the local mutation rate (μ, approximated by the
506 four-fold synonymous substitution rate) (Figure 2B, Table S11). Hence, the broad-scale
507 variation in genetic diversity is conserved across the diverging lineages, which likely
508 arise from a common genomic architecture where linked selection has played a major
509 role in shaping local genomic diversity (Burri, 2017). This is further highlighted by the
510 conserved landscape of recombination rate variation across the genomes of the species
511 and the strong degree of genome synteny that we observed between the genomes of
512 aspens and poplars (Lin et al., 2018). Second, we found that the differentiation
513 landscapes were highly correlated among all species pairs both for the relative (F_{ST}) and
514 the absolute (d_{xy}) measures of genetic differentiation (Figure 2B, Figure S9, Table S11).
515 The highly similar landscape of differentiation among different species pairs could
516 imply phylogenetically conserved genomic features, e.g. conserved landscapes of
517 functional densities and recombination (Burri, 2017; Vijay et al., 2017). Moreover,
518 significantly negative correlations between F_{ST} and π were found in all pairwise
519 comparisons (Figure 2B, Figure S9, Table S11), which is in line with the observation
520 that F_{ST} is sensitive to intra-specific nucleotide diversity (Charlesworth, 1998). In

521 contrast, only weak correlations were observed between d_{xy} and π. Because d_{xy} largely
522 reflects diversity in a common ancestor (Cruickshank & Hahn, 2014), a weak
523 correlation between d_{xy} and π implies that ancestral diversity might have little impact on
524 extant diversity in the different *Populus* species. In addition to extant diversity, d_{xy} was
525 only weakly correlated with F_{ST} across all comparisons (Figure 3B, Figure S9, Table
526 S11), which further implies that ancestral polymorphisms have had limited contribution
527 to the genomic divergence of extant species (Cruickshank & Hahn, 2014).
528
529 ***3.3 Topology weighting reveals phylogenetic discordance and ancient introgression***
530 ***between P. tremula and P. tremuloides***
531 Even if the analyses of current population structure and genomic divergence support a
532 clear species relationship for the four *Populus* species, (((*P. tremula*, *P. davidiana*), *P.*
533 *tremuloides*), *P. trichocarpa*), we used a topology weighting approach to explore to
534 what degree the 'species tree' was congruent across the entire genome. Using *P.*
535 *trichocarpa* as an outgroup, our results reveal widespread incongruence in local
536 genealogies in either 10 Kbp or 100 Kbp non-overlapping windows across the genome
537 (Figure 3, Figure S10). The most prevalent topology, ((*P. tremula*, *P. davidiana*), *P.*
538 *tremuloides*), which reflects the likely 'species topology', has an average weighting of
539 54.7% and 76.5% across the genome in 10 Kbp and 100 Kbp windows, respectively. Of
540 the other two topologies, the ((*P. tremula*, *P. tremuloides*), *P. davidiana*) topology was
541 much more common (27.0% and 17.6% for 10 Kbp and 100 Kbp windows) compared
542 to ((*P. davidiana*, *P. tremuloides*), *P. tremula*) (18.3% and 5.9% for 10 Kbp and 100
543 Kbp windows) (Figure 3, Table S12). In general, we observed that larger windows (100
544 Kbp) produced higher rates of monophyly (windows with a weighting of 1) and a

545 greater fraction of resolved trees compared to the smaller windows (10 Kbp) (Figure
546 S10, Table S13).

547 Interestingly, in contrast to all other chromosomes where all three topologies were
548 observed, chromosome 19, which is known to harbor the sex determination region in
549 *Populus* (Yin et al., 2008), showed only a single monophyletic grouping of the 'species
550 topology' (Figure 3). Such a pattern is consistent with the expectation that lineage
551 sorting is faster on sex chromosomes compared to autosomes because of its smaller
552 effective population size (Meisel & Connallon, 2013; Vicoso & Charlesworth, 2006).
553 Overall, both incomplete lineage sorting (ILS) and introgression can result in
554 discordance between the local topology and the species tree for recently diverged
555 species. Given that ILS is expected to generate equal frequencies of the alternative
556 topologies (Durand et al., 2011; Mailund et al., 2014), the more frequent topology of
557 ((*P. tremula*, *P. tremuloides*), *P. davidiana*) is likely explained by the occurrence of
558 introgression between *P. tremula* and *P. tremuloides*. We therefore compared the
559 distribution of the branch lengths separating each pair of aspen species among all
560 topology types. Compared to the expectation that species with recent introgression tend
561 to be separated by short branches (Fontaine et al., 2015; Martin & Van Belleghem,
562 2017), the branch distances between *P. tremula* and *P. tremuloides* were not obviously
563 different from other species-pairs across topology comparisons (Figure S11). This
564 pattern is most likely caused by ancient hybridization between these two species where
565 genetic drift has eradicated most signatures of gene flow after an ancient introgression
566 event (Schumer, Cui, Powell, Rosenthal, & Andolfatto, 2016).

567 To further investigate patterns of ancient introgression between *P. tremula* and *P.*
568 *tremuloides*, we calculated two statistics associated with the ABBA-BABA test across
569 the genome. The *D*-statistic is used to test for ancient gene flow by comparing the

imbalance of ABBAs and BABAs, and the f_d-statistic is used to estimate the fraction of the genome shared through ancient introgression. For the *D*-statistics, we also implemented two different approaches, which differed in whether the called genotypes was relied or not. We find that the estimates of the two approaches are highly correlated with each other (Figure S12), suggesting that this statistic is robust to identify introgression regardless of which type of data is used. Genome-wide estimates of the *D*-statistic and *f*-statistic showed a general pattern of positive values over 10 Kbp and 100 Kbp non-overlapping windows (Table S14), confirming that *P. tremuloides* has a closer genetic relationship with *P. tremula* than with *P. davidiana*. Thus, the significant asymmetry in genetic relationship together with the excess of shared sequence polymorphism between *P. tremula* and *P. tremuloides* (Figure S13) all provide evidence for historical gene flow between the currently allopatric Eurasian and North American aspen species.

3.4 Long-term effects of selection in shaping patterns of diversity, divergence, incomplete lineage sorting (ILS) and levels of introgression in Populus species

To evaluate the impact of natural selection on genetic diversity, divergence, ILS and gene flow in the context of speciation, we examined the correlations between these genetic parameters and factors affecting the extent and efficiency of selection. First, regions with a high density of potential targets for selection are expected to experience stronger linked selection simply because selection occurs more often in such regions (Al-Shahrour et al., 2010; Flowers et al., 2011). We therefore examined the relationship between intraspecific diversity, species divergence and the density of functional elements, defined as the proportion of protein-coding sites within a 10 Kbp or 100 Kbp window (coding density). We hypothesized that if selection contributes to the reduction

of diversity at linked neutral sites, its effect is expected to be more pronounced in regions with greater content of functional elements (Ravinet et al., 2017). Consistent with this prediction, we observed a significantly negative relationship between π and functional content (Figure 4A). This correlation was robust to the presence of confounding factors such as GC content, recombination rate and the choice of window size (Table S15).

Moreover, if natural selection was acting on the ancestral polymorphisms prior to the divergence of the two descendant lineages, it could also have an effect on the genetic divergence between species (Munch et al., 2016; Scally et al., 2012). We therefore examined the relationship between interspecies divergence (both F_{ST} and d_{xy}) and coding density, and observed negative relationships for both F_{ST} and d_{xy} (Figure 4B, C), especially between species with longer divergence times (e.g. aspens and *P. trichocarpa*) (Table S17, Table S19). Indeed, if a region experiences natural selection during divergence, it should show lower π within species and higher F_{ST} between species because F_{ST} is sensitive to intra-specific genetic variation (Cruickshank & Hahn, 2014). Accordingly, a positive correlation between coding density and F_{ST} is predicted. The opposite pattern we observe here indicates that long-term natural selection, most likely due to background selection in functional regions, has continuously contributed to the reduced ancestral polymorphism and genetic divergence in regions with greater functional content (Phung et al., 2016). In fact, because of the accumulation of the large amount of new mutations since speciation, ancestral polymorphism may only account for a small amount of the overall average divergence between distantly related species (Edwards & Beerli, 2000). However, the variance of ancestral polymorphism, largely affected by natural selection in ancestral populations, can on the other hand make a substantial contribution to the variability of genome-wide

patterns of divergence between species (McVicker, Gordon, Davis, & Green, 2009; Phung et al., 2016).

To further explore the role of natural selection during the divergence of the three aspen species, we examined the extent of ILS across the genome, which can aid to infer evolutionary process in ancestral populations (Mailund et al., 2014; Pease & Hahn, 2013). The pattern of ILS along the genome offers information about the local differences in the ancestral effective population size of the *aspen* ancestor (Pamilo & Nei, 1988). Both purifying and positive selection in the ancestral population are expected to reduce ancestral population size in regions targeted by selection, resulting in increased rates for lineages to coalesce and leaving less available for ILS (Dutheil, Munch, Nam, Mailund, & Schierup, 2015; Munch et al., 2016; Prüfer et al., 2012; Scally et al., 2012). In agreement with this, we found that the fraction of ILS decreases with increasing coding density (Figure 4D), and this relationship remained even after correcting for the confounding variables (Table S21). Within coding exons, ILS is ~19 % lower and the suppression of ILS extends several thousand bps away from coding genes (Figure S14). Similarly, the proportion of the topology reflecting the true species tree increases with coding density (Figure 4E; Table S21).

In addition, given that the level of admixture estimated by f_d between *P. tremula* and *P. tremuloides* show considerable heterogeneity across the genome (Figure S15), we examined whether selection may have played a role in shaping genome-wide patterns of introgression. We estimated the relationship between f_d and coding density and found a significantly negative correlation (Figure 4F; Table S21), indicating that there is greater selection against introgressed alleles in regions enriched for genes (Harris & Nielsen, 2016). The occurrence of this pattern is not likely an artefact of reduced power, as regions with a high density of functionally important elements are

expected to have experienced stronger long-term selection and exhibit lower levels of ILS. Accordingly, our power to detect introgression is expected to be elevated close to these regions (Sankararaman et al., 2014; Sankararaman, Mallick, Patterson, & Reich, 2016). Taken together, it is clear that natural selection has had a strong impact on patterns of phylogenetic discordance across the genome among closely related aspen species. However, it is not yet clear to what extent this heterogeneity might be due to incomplete lineage sorting of ancestral polymorphisms or due to ancient introgression. More explicit experimental designs in future studies are needed to tease apart these different processes and explore how natural selection and hybridization act in combination to shape the genome-wide phylogenetic heterogeneity among recently diverged species.

In addition to the local density of functional elements, recombination rates can also interact with natural selection to influence the genomic distribution of genetic diversity and divergence (Figure 4). High recombination can rapidly decouple linked loci and restrict the effect of selection on linked neutral sites (Begun & Aquadro, 1992; Cutter & Payseur, 2013). We found that π and F_{ST} showed positive and negative correlations, respectively, with local recombination rates (Figure 4A-C; Table S16, S18, S20). In contrast to the predicted pattern of speciation with gene flow where reduced d_{xy} is expected in regions of high recombination (Nachman & Payseur, 2012), we did not find any relationship between d_{xy} and recombination rate. These observations are in accordance with the expectation that linked selection is prevalent and has genome-wide effects in shaping patterns of genetic diversity and divergence at linked sites in *Populus* (Nachman & Payseur, 2012; Wang et al., 2016b). On the other hand, we found that the incidence of ILS increases with the recombination rate (Figure 4D), which was still observable even after correcting for the confounding variables of coding density and

GC content (Table S22). Given that variation in ILS across the genome approximately reflects variation in ancestral N_e (Degnan & Salter, 2005; Pamilo & Nei, 1988), the stronger effects of recurrent natural selection in low-recombination regions also reduced N_e in ancestral populations and hence made ILS less likely to occur (Charlesworth et al., 1993; Martin, Davey, Salazar, & Jiggins, 2019; Pease & Hahn, 2013). We did not find obvious correlation between f_d and recombination rate (Figure 4F, Table S22), might because barriers to introgression has been sculpted by long-term selection and genetic drift after the ancient gene flow and cannot be predicted by recombination rate estimated from current populations. Overall, all these results suggest that the patterns of diversity, divergence and genealogical relationships among the three closely related aspen species are not randomly distributed along the genome, but instead are strongly structured by the interaction between widespread natural selection and intrinsic genomic features, as well as their influence on retention of signatures of ancient gene flow.

3.5 The impact of positive and balancing selection on genomic architecture of speciation

Although widespread background selection is likely to have had a large effect in shaping the heterogeneous genomic landscape of variation within and between species (Burri, 2017; Charlesworth, 2012), we were interested in assessing whether positive selection or long-term balancing selection have also played important roles in driving these processes. To identify the impact of positive selection, we performed a composite-likelihood based (CLR) test to scan the genomes for signals of positive selection in each of the three aspen species (Figure 5A). For each species, we considered the windows with a CLR value in the top 1 percentile as candidate region under positive selection. In total, we detected 538 outlier windows across the three

695 species, and only 13 among them were shared by all species (Figure 5B). Our results
696 suggest that most putative sweeps are likely species-specific and may result from
697 relatively recent positive selection that has occurred independently in various lineages
698 after speciation. Compared to genome-wide averages, outlier windows have
699 significantly lower nucleotide diversity, lower recombination rates, higher F_{ST} but
700 similar d_{xy} (Figure 5C). In addition, the outlier windows show significantly higher
701 average weightings of the 'species topology' (Topo2) and lower levels of ILS compared
702 to genomic background (Figure 5C,D). The ancestral admixture proportion (f_d) between
703 *P. tremula* and *P. tremuloides* is also significantly reduced in the outlier windows
704 (Figure 5D), suggesting that strong selection in these regions may have contributed to
705 the reproductive barriers isolating closely related species (Martin et al., 2019).

706 To further study how long-term balancing selection may have driven the evolution
707 of the genomic landscape during speciation, we used a summary statistics, β (beta score),
708 to search for signals of balancing selection across the genome for each aspen species
709 (Siewert & Voight, 2017). As we did for positive selection, we only consider variants
710 with β scores falling in the top 1% as candidate variants. Furthermore, variants
711 simultaneously detected in all three species are considered as potential targets of
712 long-term balancing selection. With this criteria we identified a total of 519 variants
713 putatively under long-term balancing selection across the three aspen species (Figure
714 6A,B). These variants were unevenly distributed in the genome, and to make them
715 comparable to our previous analyses we clustered them into 32 regions of 10 Kbp
716 windows (Figure 6A). We found significantly higher nucleotide diversity, higher
717 recombination rates, lower F_{ST}, and higher d_{xy} in the regions under balancing selection
718 compared to the genomic background (Figure 6C). Moreover, we found lower
719 weightings of the 'species topology', higher ILS, and lower f_d in the candidate balancing

720 selection regions although the results were not significant, likely due to the small
721 number of windows showing evidence for balancing selection (Figure 6C,D). We
722 therefore infer that long-term balancing selection may not only influence the genomic
723 landscape of diversity and divergence but may also play a role in shaping the
724 genealogical relationship and barriers to introgression among closely related species
725 (Charlesworth, 2006; Wang et al., 2019).

726 Finally, to assess whether there were any specific biological functions that were
727 significantly over-represented on genes located in regions identified as undergoing
728 either positive (506 genes) or long-term balancing selection (32 genes), we performed
729 gene ontology (GO) enrichment analysis. We did not detect over-representation for any
730 functional category among the candidate genes under long-term balancing selection. In
731 contrast, we identified 31 significantly enriched GO categories (Fisher's exact test,
732 $P<0.01$) for genes under positive selection (Table S23). These GO clusters were
733 primarily associated with metabolic processes (DNA, nucleic acid, cellular
734 macromolecule and aromatic compound, molybdopterin confactor), biosynthetic
735 processes (molybdopterin confactor, vitamin B6), cell morphogenesis and gene
736 expression regulation. Together these functional clusters are biologically relevant for
737 plant adaptation, because the biosynthesis of a panoply of diverse natural chemicals
738 serve as important adaptive strategies for sessile long-lived trees to adapt to
739 ever-changing abiotic and biotic environments (Weng, 2014).

740

741 ## 4. Discussion

742 Much of our knowledge of how genomic landscape builds in the speciation process is
743 drawn from studies focusing on two young species pairs with ongoing gene flow. Very
744 few examples of now-allopatric species pairs along the speciation continuum have been

745 investigated. Here, we focus our research on four widespread *Populus* species that are
746 allopatrically distributed in northern Hemisphere. After characterizing their speciation
747 and demographic histories, we find that species in different continent exhibited
748 idiosyncratic responses to Pleistocene climate changes. In addition, ancient gene flow
749 was detected between extant Eurasian and North American aspen species (*P. tremula*
750 and *P. tremuloides*). We also investigated the evolutionary forces that have shaped
751 genome-wide patterns of variations within and between species. Our results have found
752 substantial variation in genetic diversity, divergence, species relationships and the
753 extent of introgression along the genome. Variation in these patterns is predictable and
754 can be largely explained by genome-wide variation in the strength and extent of both
755 recent and ancient selection, which depends on the recombination rate and the local
756 density of functional sites. Our findings therefore provide evidence of how recurrent
757 selection interacts with genomic features to shape the genomic landscape during species
758 divergence. We further demonstrate that not only background selection, positive and
759 long-term balancing selection also play crucial roles in shaping genomic variation and
760 phylogenetic relationship among the recently diverged aspen species. Overall, this study
761 highlights the striking impacts of natural selection in shaping within- and between-
762 species genomic variation through speciation.
763

764 ## Acknowlegements

765 All analyses were performed on resources provided by the Swedish National
766 Infrastructure for Computing (SNIC) at Uppsala Multidisciplinary Center for Advanced
767 Computational Science (UPPMAX) under the projects SNIC2016-7-89 and SNIC
768 2017/1-499. Financial support was provided by National Natural Science Foundation of
769 China (31971567) and the Fundamental Research Funds for the Central Universities.

References

Abbott, R., Albach, D., Ansell, S., Arntzen, J. W., Baird, S. J., Bierne, N., . . . Buggs, R. (2013). Hybridization and speciation. *Journal of Evolutionary Biology, 26*(2), 229-246.

Al-Shahrour, F., Minguez, P., Marqués-Bonet, T., Gazave, E., Navarro, A., & Dopazo, J. (2010). Selection upon genome architecture: conservation of functional neighborhoods with changing genes. *PLoS Computational Biology, 6*(10), e1000953.

Alexa, A., & Rahnenführer, J. (2009). Gene set enrichment analysis with topGO. *Bioconductor Improv*, 27.

Bai, W. N., Yan, P. C., Zhang, B. W., Woeste, K. E., Lin, K., & Zhang, D. Y. (2018). Demographically idiosyncratic responses to climate change and rapid Pleistocene diversification of the walnut genus Juglans (Juglandaceae) revealed by whole-genome sequences. *New Phytologist, 217*(4), 1726-1736.

Begun, D. J., & Aquadro, C. F. (1992). Levels of naturally occurring DNA polymorphism correlate with recombination rates in D. melanogaster. *Nature, 356*(6369), 519.

Browning, B. L., & Browning, S. R. (2009). A unified approach to genotype imputation and haplotype-phase inference for large data sets of trios and unrelated individuals. *The American Journal of Human Genetics, 84*(2), 210-223.

Browning, B. L., & Browning, S. R. (2013). Improving the accuracy and efficiency of identity-by-descent detection in population data. *Genetics, 194*(2), 459-471.

Burri, R. (2017). Interpreting differentiation landscapes in the light of long-term linked selection. *Evolution Letters, 1*(3), 118-131.

Burri, R., Nater, A., Kawakami, T., Mugal, C. F., Olason, P. I., Smeds, L., . . . Garamszegi, L. Z. (2015). Linked selection and recombination rate variation drive the evolution of the genomic landscape of differentiation across the speciation continuum of Ficedula flycatchers. *Genome Research, 25*(11), 1656-1665.

Chan, A. H., Jenkins, P. A., & Song, Y. S. (2012). Genome-wide fine-scale recombination rate variation in Drosophila melanogaster. *PLoS Genetics, 8*(12), e1003090.

Charlesworth, B. (1998). Measures of divergence between populations and the effect of forces that reduce variability. *Molecular Biology and Evolution, 15*(5), 538-543.

Charlesworth, B. (2012). The effects of deleterious mutations on evolution at linked sites. *Genetics, 190*(1), 5-22.

Charlesworth, B., Morgan, M., & Charlesworth, D. (1993). The effect of deleterious mutations on neutral molecular variation. *Genetics, 134*(4), 1289-1303.

Charlesworth, D. (2006). Balancing selection and its effects on sequences in nearby genome regions. *PLoS Genetics, 2*(4), e64.

Comeron, J. M., Williford, A., & Kliman, R. (2008). The Hill–Robertson effect: evolutionary consequences of weak selection and linkage in finite populations. *Heredity, 100*(1), 19.

Cruickshank, T. E., & Hahn, M. W. (2014). Reanalysis suggests that genomic islands of speciation are due to reduced diversity, not reduced gene flow. *Molecular Ecology, 23*(13), 3133-3157.

Cutter, A. D., & Payseur, B. A. (2013). Genomic signatures of selection at linked sites: unifying the disparity among species. *Nature Reviews Genetics, 14*(4), 262.

Danecek, P., Auton, A., Abecasis, G., Albers, C. A., Banks, E., DePristo, M. A., . . . Sherry, S. T. (2011). The variant call format and VCFtools. *Bioinformatics, 27*(15), 2156-2158.

DeGiorgio, M., Huber, C. D., Hubisz, M. J., Hellmann, I., & Nielsen, R. (2016). SweepFinder2: increased sensitivity, robustness and flexibility. *Bioinformatics, 32*(12), 1895-1897.

Degnan, J. H., & Salter, L. A. (2005). Gene tree distributions under the coalescent process. *Evolution, 59*(1), 24-37.

Delmore, K. E., Lugo Ramos, J. S., Van Doren, B. M., Lundberg, M., Bensch, S., Irwin, D. E., & Liedvogel, M. (2018). Comparative analysis examining patterns of genomic differentiation across multiple episodes of population divergence in birds. *Evolution Letters, 2*(2), 76-87.

DePristo, M. A., Banks, E., Poplin, R., Garimella, K. V., Maguire, J. R., Hartl, C., . . . Hanna, M. (2011). A framework for variation discovery and genotyping using next-generation DNA sequencing data. *Nature Genetics, 43*(5), 491.

Du, S., Wang, Z., Ingvarsson, P. K., Wang, D., Wang, J., Wu, Z., . . . Zhang, J. (2015). Multilocus analysis of nucleotide variation and speciation in three closely related P opulus (S alicaceae) species. *Molecular Ecology, 24*(19), 4994-5005.

Durand, E. Y., Patterson, N., Reich, D., & Slatkin, M. (2011). Testing for ancient admixture between closely related populations. *Molecular Biology and Evolution, 28*(8), 2239-2252.

Dutheil, J. Y., Munch, K., Nam, K., Mailund, T., & Schierup, M. H. (2015). Strong selective sweeps on the X chromosome in the human-chimpanzee ancestor explain its low divergence. *PLoS Genetics, 11*(8), e1005451.

Eckenwalder, J. E. (1996). Systematics and evolution of Populus. *Biology of Populus and its Implications for Management and Conservation, 7*, 32.

Edwards, S., & Beerli, P. (2000). Perspective: gene divergence, population divergence, and the variance in coalescence time in phylogeographic studies. *Evolution, 54*(6), 1839-1854.

Ellegren, H., & Galtier, N. (2016). Determinants of genetic diversity. *Nature Reviews Genetics, 17*(7), 422.

Excoffier, L., Dupanloup, I., Huerta-Sánchez, E., Sousa, V. C., & Foll, M. (2013). Robust demographic inference from genomic and SNP data. *PLoS Genetics, 9*(10), e1003905.

Feder, J. L., Egan, S. P., & Nosil, P. (2012). The genomics of speciation-with-gene-flow. *Trends in Genetics, 28*(7), 342-350.

Flaxman, S. M., Wacholder, A. C., Feder, J. L., & Nosil, P. (2014). Theoretical models of the influence of genomic architecture on the dynamics of speciation. *Molecular Ecology, 23*(16), 4074-4088.

Flowers, J. M., Molina, J., Rubinstein, S., Huang, P., Schaal, B. A., & Purugganan, M. D. (2011). Natural selection in gene-dense regions shapes the genomic pattern of polymorphism in wild and domesticated rice. *Molecular Biology and Evolution, 29*(2), 675-687.

Fontaine, M. C., Pease, J. B., Steele, A., Waterhouse, R. M., Neafsey, D. E., Sharakhov, I. V., . . . Kakani, E. (2015). Extensive introgression in a malaria vector species complex revealed by phylogenomics. *Science, 347*(6217), 1258524.

Fumagalli, M., Vieira, F. G., Korneliussen, T. S., Linderoth, T., Huerta-Sánchez, E., Albrechtsen, A., & Nielsen, R. (2013). Quantifying population genetic differentiation from next-generation sequencing data. *Genetics*, *195*(3), 979-992.

Fumagalli, M., Vieira, F. G., Linderoth, T., & Nielsen, R. (2014). ngsTools: methods for population genetics analyses from next-generation sequencing data. *Bioinformatics*, *30*(10), 1486-1487.

Gao, Z., Przeworski, M., & Sella, G. (2015). Footprints of ancient - balanced polymorphisms in genetic variation data from closely related species. *Evolution*, *69*(2), 431-446.

Green, R. E., Krause, J., Briggs, A. W., Maricic, T., Stenzel, U., Kircher, M., . . . Fritz, M. H.-Y. (2010). A draft sequence of the Neandertal genome. *Science*, *328*(5979), 710-722.

Guerrero, R. F., & Hahn, M. W. (2017). Speciation as a sieve for ancestral polymorphism. *Molecular Ecology*, *26*(20), 5362-5368.

Hamzeh, M., & Dayanandan, S. (2004). Phylogeny of Populus (Salicaceae) based on nucleotide sequences of chloroplast TRNT-TRNF region and nuclear rDNA. *American Journal of Botany*, *91*(9), 1398-1408.

Han, F., Lamichhaney, S., Grant, B. R., Grant, P. R., Andersson, L., & Webster, M. T. (2017). Gene flow, ancient polymorphism, and ecological adaptation shape the genomic landscape of divergence among Darwin's finches. *Genome Research*, *27*(6), 1004-1015.

Harris, K., & Nielsen, R. (2016). The genetic cost of Neanderthal introgression. *Genetics*, *203*(2), 881-891.

Hart, J., De Araujo, F., Thomas, B., & Mansfield, S. (2013). Wood quality and growth characterization across intra-and inter-specific hybrid aspen clones. *Forests*, *4*(4), 786-807.

Hobolth, A., Dutheil, J. Y., Hawks, J., Schierup, M. H., & Mailund, T. (2011). Incomplete lineage sorting patterns among human, chimpanzee, and orangutan suggest recent orangutan speciation and widespread selection. *Genome Research*, *21*(3), 349-356.

Hudson, R. R., & Kaplan, N. L. (1995). Deleterious background selection with recombination. *Genetics*, *141*(4), 1605-1617.

Hurst, L. D., Pál, C., & Lercher, M. J. (2004). The evolutionary dynamics of eukaryotic gene order. *Nature Reviews Genetics*, *5*(4), 299.

Jansson, S., & Douglas, C. J. (2007). Populus: a model system for plant biology. *Annual Review of Plant Biology*, *58*, 435-458.

Kaplan, N. L., Hudson, R., & Langley, C. (1989). The" hitchhiking effect" revisited. *Genetics*, *123*(4), 887-899.

Koch, M. A., Haubold, B., & Mitchell-Olds, T. (2000). Comparative evolutionary analysis of chalcone synthase and alcohol dehydrogenase loci in Arabidopsis, Arabis, and related genera (Brassicaceae). *Molecular Biology and Evolution*, *17*(10), 1483-1498.

Korneliussen, T. S., Albrechtsen, A., & Nielsen, R. (2014). ANGSD: analysis of next generation sequencing data. *BMC Bioinformatics*, *15*(1), 356.

Lamichhaney, S., Berglund, J., Almén, M. S., Maqbool, K., Grabherr, M., Martinez-Barrio, A., . . . Zamani, N. (2015). Evolution of Darwin’s finches and their beaks revealed by genome sequencing. *Nature*, *518*(7539), 371.

Lee, T.-H., Guo, H., Wang, X., Kim, C., & Paterson, A. H. (2014). SNPhylo: a pipeline to construct a phylogenetic tree from huge SNP data. *BMC Genomics*, *15*(1), 162.

Li, H. (2013). Aligning sequence reads, clone sequences and assembly contigs with BWA-MEM. *arXiv:1303.3997*.

Li, H., & Durbin, R. (2009). Fast and accurate short read alignment with Burrows–Wheeler transform. *Bioinformatics*, *25*(14), 1754-1760.

Li, H., Handsaker, B., Wysoker, A., Fennell, T., Ruan, J., Homer, N., . . . Durbin, R. (2009). The sequence alignment/map format and SAMtools. *B ioinformatics*, *25*(16), 2078-2079.

Lin, Y.-C., Wang, J., Delhomme, N., Schiffthaler, B., Sundström, G., Zuccolo, A., . . . Cossu, R. M. (2018). Functional and evolutionary genomic inferences in Populus through genome and population sequencing of American and European aspen. *Proceedings of the National Academy of Sciences*, *115*(46), E10970-E10978.

Lohmueller, K. E., Albrechtsen, A., Li, Y., Kim, S. Y., Korneliussen, T., Vinckenbosch, N., . . . Grarup, N. (2011). Natural selection affects multiple aspects of genetic variation at putatively neutral sites across the human genome. *PLoS Genetics*, *7*(10), e1002326.

Lohse, M., Bolger, A. M., Nagel, A., Fernie, A. R., Lunn, J. E., Stitt, M., & Usadel, B. (2012). R obi NA: A user-friendly, integrated software solution for RNA-Seq-based transcriptomics. *Nucleic Acids Research*, *40*(W1), W622-W627.

Ma, T., Wang, K., Hu, Q., Xi, Z., Wan, D., Wang, Q., . . . Abbott, R. J. (2018). Ancient polymorphisms and divergence hitchhiking contribute to genomic islands of divergence within a poplar species complex. *Proceedings of the National Academy of Sciences*, *115*(2), E236-E243.

Mailund, T., Munch, K., & Schierup, M. H. (2014). Lineage sorting in apes. *Annual Review of Genetics*, *48*, 519-535.

Martin, S. H., Davey, J. W., & Jiggins, C. D. (2014). Evaluating the use of ABBA–BABA statistics to locate introgressed loci. *Molecular Biology and Evolution*, *32*(1), 244-257.

Martin, S. H., Davey, J. W., Salazar, C., & Jiggins, C. D. (2019). Recombination rate variation shapes barriers to introgression across butterfly genomes. *PLoS Biology*, *17*(2), e2006288.

Martin, S. H., & Van Belleghem, S. M. (2017). Exploring evolutionary relationships across the genome using topology weighting. *Genetics*, *206*(1), 429-438.

Matthey-Doret, R., & Whitlock, M. C. (2019). Background selection and FST: consequences for detecting local adaptation. *Molecular Ecology*. doi: 10.1111/mec.15197.

McVicker, G., Gordon, D., Davis, C., & Green, P. (2009). Widespread genomic signatures of natural selection in hominid evolution. *PLoS Genetics*, *5*(5), e1000471.

Meisel, R. P., & Connallon, T. (2013). The faster-X effect: integrating theory and data. *Trends in genetics*, *29*(9), 537-544.

Munch, K., Nam, K., Schierup, M. H., & Mailund, T. (2016). Selective sweeps across twenty millions years of primate evolution. *Molecular Biology and Evolution*, *33*(12), 3065-3074.

Nachman, M. W., & Payseur, B. A. (2012). Recombination rate variation and speciation: theoretical predictions and empirical results from rabbits and mice.

963 *Philosophical Transactions of the Royal Society B: Biological Sciences*,
964 *367*(1587), 409-421.
965 Nadachowska-Brzyska, K., Burri, R., Olason, P. I., Kawakami, T., Smeds, L., &
966 Ellegren, H. (2013). Demographic divergence history of pied flycatcher and
967 collared flycatcher inferred from whole-genome re-sequencing data. *PLoS*
968 *Genetics*, *9*(11), e1003942.
969 Nadeau, N. J., Whibley, A., Jones, R. T., Davey, J. W., Dasmahapatra, K. K., Baxter, S.
970 W., . . . Blaxter, M. L. (2012). Genomic islands of divergence in hybridizing
971 Heliconius butterflies identified by large-scale targeted sequencing.
972 *Philosophical Transactions of the Royal Society B: Biological Sciences*,
973 *367*(1587), 343-353.
974 Neale, D. B., & Ingvarsson, P. K. (2008). Population, quantitative and comparative
975 genomics of adaptation in forest trees. *Current opinion in plant biology*, *11*(2),
976 149-155.
977 Neale, D. B., & Kremer, A. (2011). Forest tree genomics: growing resources and
978 applications. *Nature Reviews Genetics*, *12*(2), 111.
979 Nielsen, R., Korneliussen, T., Albrechtsen, A., Li, Y., & Wang, J. (2012). SNP calling,
980 genotype calling, and sample allele frequency estimation from new-generation
981 sequencing data. *PloS One*, *7*(7), e37558.
982 Nordborg, M., Hu, T. T., Ishino, Y., Jhaveri, J., Toomajian, C., Zheng, H., . . . Goyal, R.
983 (2005). The pattern of polymorphism in Arabidopsis thaliana. *PLoS Biology*,
984 *3*(7), e196.
985 Nosil, P., Funk, D. J., & Ortiz-Barrientos, D. (2009). Divergent selection and
986 heterogeneous genomic divergence. *Molecular Ecology*, *18*(3), 375-402.
987 Pamilo, P., & Nei, M. (1988). Relationships between gene trees and species trees.
988 *Molecular Biology and Evolution*, *5*(5), 568-583.
989 Patterson, N., Price, A. L., & Reich, D. (2006). Population structure and eigenanalysis.
990 *PLoS Genetics*, *2*(12), e190.
991 Pease, J. B., & Hahn, M. W. (2013). More accurate phylogenies inferred from low-
992 recombination regions in the presence of incomplete lineage sorting. *Evolution*,
993 *67*(8), 2376-2384.
994 Phung, T. N., Huber, C. D., & Lohmueller, K. E. (2016). Determining the effect of
995 natural selection on linked neutral divergence across species. *PLoS Genetics*,
996 *12*(8), e1006199.
997 Prüfer, K., Munch, K., Hellmann, I., Akagi, K., Miller, J. R., Walenz, B., . . . Winer, R.
998 (2012). The bonobo genome compared with the chimpanzee and human
999 genomes. *Nature*, *486*(7404), 527.
1000 Ravinet, M., Faria, R., Butlin, R., Galindo, J., Bierne, N., Rafajlović, M., . . . Westram,
1001 A. (2017). Interpreting the genomic landscape of speciation: a road map for
1002 finding barriers to gene flow. *Journal of Evolutionary Biology*, *30*(8),
1003 1450-1477.
1004 Ravinet, M., Yoshida, K., Shigenobu, S., Toyoda, A., Fujiyama, A., & Kitano, J.
1005 (2018). The genomic landscape at a late stage of stickleback speciation: High
1006 genomic divergence interspersed by small localized regions of introgression.
1007 *PLoS Genetics*, *14*(5), e1007358.
1008 Sankararaman, S., Mallick, S., Dannemann, M., Prüfer, K., Kelso, J., Pääbo, S., . . .
1009 Reich, D. (2014). The genomic landscape of Neanderthal ancestry in present-day
1010 humans. *Nature*, *507*(7492), 354.

Sankararaman, S., Mallick, S., Patterson, N., & Reich, D. (2016). The combined landscape of Denisovan and Neanderthal ancestry in present-day humans. *Current Biology*, *26*(9), 1241-1247.

Scally, A., Dutheil, J. Y., Hillier, L. W., Jordan, G. E., Goodhead, I., Herrero, J., . . . Marques-Bonet, T. (2012). Insights into hominid evolution from the gorilla genome sequence. *Nature*, *483*(7388), 169.

Schiffels, S., & Durbin, R. (2014). Inferring human population size and separation history from multiple genome sequences. *Nature Genetics*, *46*(8), 919.

Schumer, M., Cui, R., Powell, D. L., Rosenthal, G. G., & Andolfatto, P. (2016). Ancient hybridization and genomic stabilization in a swordtail fish. *Molecular Ecology*, *25*(11), 2661-2679.

Seehausen, O., Butlin, R. K., Keller, I., Wagner, C. E., Boughman, J. W., Hohenlohe, P. A., . . . Brännström, Å. (2014). Genomics and the origin of species. *Nature Reviews Genetics*, *15*(3), 176.

Siewert, K. M., & Voight, B. F. (2017). Detecting long-term balancing selection using allele frequency correlation. *Molecular biology and evolution*, *34*(11), 2996-3005.

Smith, J. M., & Haigh, J. (1974). The hitch-hiking effect of a favourable gene. *Genetics Research*, *23*(1), 23-35.

Stamatakis, A. (2014). RAxML version 8: a tool for phylogenetic analysis and post-analysis of large phylogenies. *Bioinformatics*, *30*(9), 1312-1313.

Stankowski, S., Chase, M. A., Fuiten, A. M., Rodrigues, M. F., Ralph, P. L., & Streisfeld, M. A. (2019). Widespread selection and gene flow shape the genomic landscape during a radiation of monkeyflowers. *PLoS Biology*, *17*(7), e3000391.

Tarailo-Graovac, M., & Chen, N. (2009). Using RepeatMasker to identify repetitive elements in genomic sequences. *Current Protocols in Bioinformatics*, *25*(1), 4.10. 11-14.10. 14.

Turner, T. L., Hahn, M. W., & Nuzhdin, S. V. (2005). Genomic islands of speciation in Anopheles gambiae. *PLoS Biology*, *3*(9), e285.

Tuskan, G. A., Difazio, S., Jansson, S., Bohlmann, J., Grigoriev, I., Hellsten, U., . . . Salamov, A. (2006). The genome of black cottonwood, Populus trichocarpa (Torr. & Gray). *Science*, *313*(5793), 1596-1604.

Van Doren, B. M., Campagna, L., Helm, B., Illera, J. C., Lovette, I. J., & Liedvogel, M. (2017). Correlated patterns of genetic diversity and differentiation across an avian family. *Molecular Ecology*, *26*(15), 3982-3997.

Vicoso, B., & Charlesworth, B. (2006). Evolution on the X chromosome: unusual patterns and processes. *Nature Reviews Genetics*, *7*(8), 645.

Vijay, N., Weissensteiner, M., Burri, R., Kawakami, T., Ellegren, H., & Wolf, J. B. (2017). Genomewide patterns of variation in genetic diversity are shared among populations, species and higher - order taxa. *Molecular Ecology*, *26*(16), 4284-4295.

Wang, B., Mojica, J. P., Perera, N., Lee, C.-R., Lovell, J. T., Sharma, A., . . . Rokhsar, D. S. (2019). Ancient polymorphisms contribute to genome-wide variation by long-term balancing selection and divergent sorting in Boechera stricta. *Genome Biology*, *20*(1), 126.

Wang, J., Street, N. R., Scofield, D. G., & Ingvarsson, P. K. (2016a). Natural selection and recombination rate variation shape nucleotide polymorphism across the genomes of three related Populus species. *Genetics*, *202*(3), 1185-1200.

Wang, J., Street, N. R., Scofield, D. G., & Ingvarsson, P. K. (2016b). Variation in linked selection and recombination drive genomic divergence during allopatric speciation of European and American aspens. *Molecular Biology and Evolution, 33*(7), 1754-1767.

Weng, J. K. (2014). The evolutionary paths towards complexity: a metabolic perspective. *New Phytologist, 201*(4), 1141-1149.

Wolf, J. B., & Ellegren, H. (2017). Making sense of genomic islands of differentiation in light of speciation. *Nature Reviews Genetics, 18*(2), 87.

Wu, C. I. (2001). The genic view of the process of speciation. *Journal of Evolutionary Biology, 14*(6), 851-865.

Yin, T., DiFazio, S. P., Gunter, L. E., Zhang, X., Sewell, M. M., Woolbright, S. A., . . . Wang, M. (2008). Genome structure and emerging evidence of an incipient sex chromosome in Populus. *Genome Research, 18*(3), 422-430.

Data Accessibility Statement

Raw whole genome resequencing data generated for this study have been deposited in the NCBI short read archive under accession number PRJNA576115

Author Contributions

J.W. conceived the study, analyzed the data and wrote the manuscript. E.J.P. provided the materials of *P. davidiana* used in this study. N.R.S., J.L., P.K.I. read and commented on the manuscript. All authors approved the final manuscript.

Figure legends:

Figure 1. Phylogenetic and population genetic analyses of four *Populus* species. (A) Sampling locations (black circle) of eight individuals from each of the four *Populus* species included in this study. Species ranges for *P. tremula*, *P. davidiana*, *P. tremuloides* and *P. trichocarpa* are indicated by red, green, blue and purple shading, respectively. (B) Maximum-likelihood phylogenetic tree reconstructed based on complete chloroplast sequences. Color scheme for the four species is the same in A-C. (C) Historical effective population size of the four *Populus* species inferred using MSMC v2 based on sets of eight haplotypes, with solid lines representing medians and shading representing ± standard deviation calculated across pairs of haplotypes. Yellow bar indicates Early Pleistocene cooling; Glacial and interglacial periods of the Late and Middle Pleistocene are indicated by dark and light grey bars, respectively; black bar indicates the period of Last Glacial Maximum (LGM). (D) Schematic of demographic scenarios of the three aspen species modeled using fastsimcoal2. The ancestral population is shown in light and dark grey respectively for different ancestral lineages. *P. tremula* is in red, *P. davidiana* is in green, and *P. tremuloides* is in blue. The arrows indicate the per generation migration rate (*m*) between species. Estimated divergence time, effective population size, and gene flow are detailed in Supplementary Table S7.

Figure 2. Genome-wide landscape of genetic diversity and divergence within and between species. (A) Chromosomal landscape of (a) the density of coding sequences (CD); (b) nucleotide diversity (π); (c) recombination rate (ρ); (d) the relative measure of genetic divergence (F_{ST}) and (e) the absolute measure of genetic divergence (d_{xy}). (B) Distribution of correlation coefficients (Spearman's ρ) shown as violin plots for population summary statistics characterizing genomic features (neutral mutation rate μ) and variation within (π, ρ) and between species (F_{ST}, d_{xy}) calculated at 100 Kbp windows. Subscripts 'i, j' symbolize all possible combinations of correlations between two species i=1…(n-1) and j=(i+1)…n for within-species measures; Capital letters 'I, J' symbolize inter-species statistics. Correlations exclude pseudo-replicated species comparisons. Detailed information can be found in Supplementary Table S11.

Figure 3. Heterogeneous distribution of phylogenies in three aspen species. Chromoplots for 19 chromosomes show the distribution of three possible rooted phylogenetic relationships inferred from 100 Kbp genomic regions for *P. tremula* (*P. tra*), *P. davidiana* (*P. dav*) and *P. tremuloides* (*P. trs*), with *P. trichocarpa* as outgroup species. The colored vertical bars represent the windows with complete monophyly of the three alternative topologies as shown in the lower right, where the proportion of the three topologies in 100 Kbp and 10 Kbp (in parenthesis) across the genome are also shown. Across all chromosomes, the *D* statistic generally tends toward positive values, indicating ancient introgression between *P. tra* and *P. trs* may have been occurring across the genome.

Figure 4. Widespread impact of linked selection. Relationship between recombination rate (blue), coding density (red) and (A) genetic diversity, (B) F_{ST}, (C) d_{xy}, (D) incomplete lineage sorting (ILS), (E) weighting of the 'species' tree ([*P. tra*, *P. dav*], *P. trs*)) and (F) the estimated admixture proportion (f_d) between *P. tra* and *P. trs*. Quantile binning is for visualization. The points and error bars indicate the means and 1.96×standard errors. Statistical tests were performed on the unbinned data and detailed correlation coefficients are shown in supplementary Table S15-Table S22.

Figure 5. Identification of positive selection. (A) Positive selection analysis by SweepFinder2 reveals windows that are candidates for being under positive selection in the three aspen species: *P. tremula* (*P. tra*), *P. davidiana* (*P. dav*) and *P. tremuloides* (*P. trs*). Horizonal red line indicates the cut-off of composite likelihood ratio (CLR) statistics. (B) The Venn diagram represents shared and unique selected windows detected in the three species. (C) Comparison of genetic diversity, recombination rate, F_{ST}, d_{xy}, and average weightings of the 'species' topology between candidate regions under positive selection (red boxes) and genomic background (grey boxes). (D) Comparison of incomplete lineage sorting (ILS) and the estimated admixture proportion (f_d)) between candidate regions under positive selection (red boxes) and genomic background (grey boxes). Asterisks designate significant differences between candidate positive selected regions and the rest of genomic regions by Mann-Whitney *U*-test ($^{n.s.}$ Not significant; * *P* value<0.01; ** *P* value<0.001; *** *P* value <1e-4).

Figure 6. Identification of long-term balancing selection. (A) Signals of balancing selection across all chromosomes in the three aspen species: *P. tremula* (*P. tra*), *P. davidiana* (*P. dav*) and *P. tremuloides* (*P. trs*). Horizonal red line indicates the cut-off of the β statistics. Only the signals detected in all three aspen species (red dots) were considered as being under long-term balancing selection. (B) The Venn diagram represents shared and unique selected SNPs detected in the three species. (C) Comparison of genetic diversity, recombination rate, F_{ST}, d_{xy}, and average weightings of the 'species' topology between candidate regions under long-term balancing selection (red boxes) and genomic background (grey boxes). (D) Comparison of incomplete lineage sorting (ILS) and the estimated admixture proportion (f_d)) between candidate regions under long-term balancing selection (red boxes) and genomic background (grey boxes). Asterisks designate significant differences between candidate balancing selected regions and the rest of genomic regions by Mann-Whitney *U*-test ($^{n.s.}$ Not significant; * *P* value<0.01; ** *P* value<0.001; *** *P* value <1e-4).

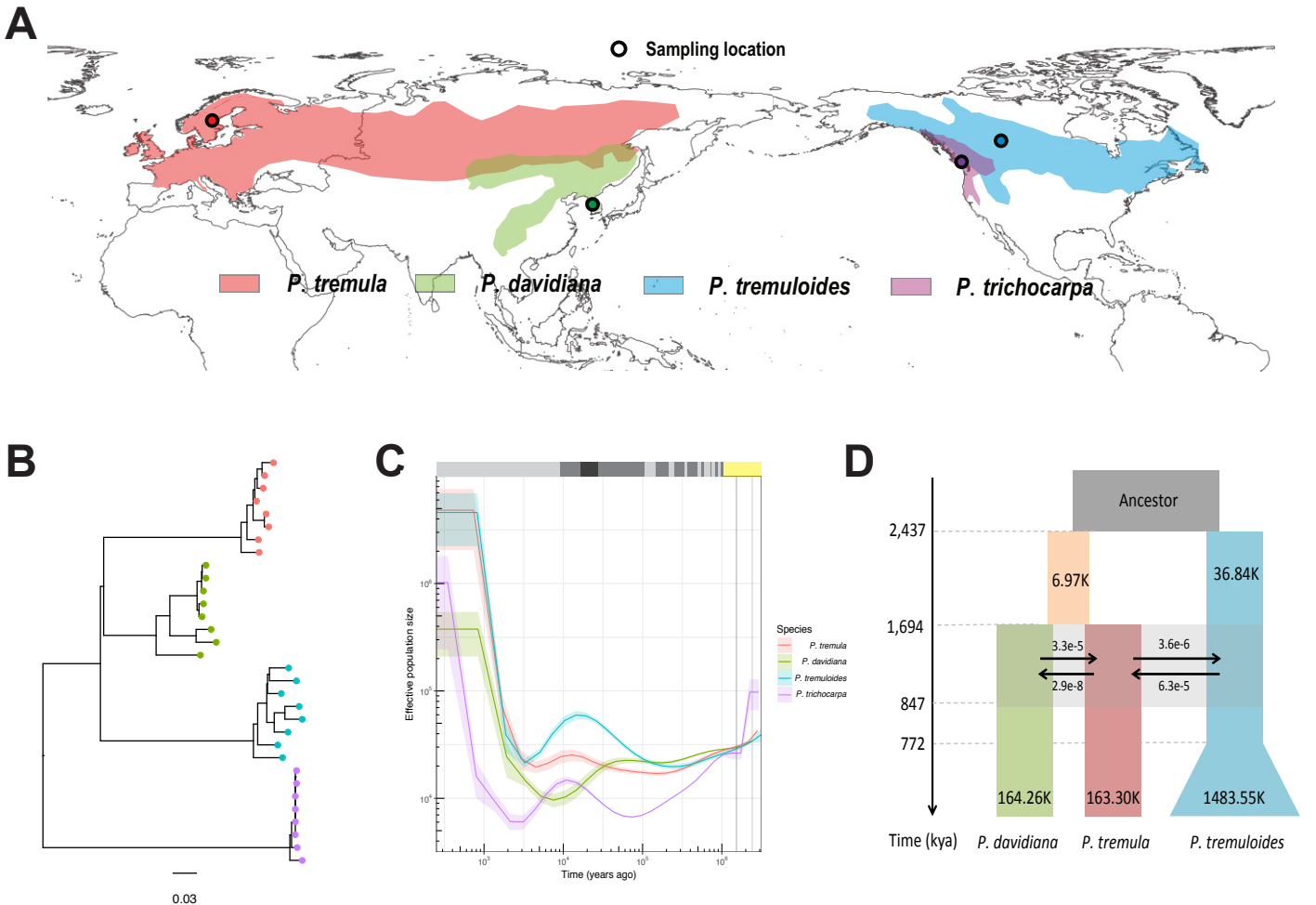
A
Sampling location
P. tremula
P. davidiana
P. tremuloides
P. trichocarpa
B
0.03
C
Effective population size
Time (years ago)
Species
P. tremula
P. davidiana
P. tremuloides
P. trichocarpa
D
Ancestor
2,437
1,694
847
772
6.97K
36.84K
3.3e-5
2.9e-8
3.6e-6
6.3e-5
164.26K
163.30K
1483.55K
Time (kya)
P. davidiana
P. tremula
P. tremuloides

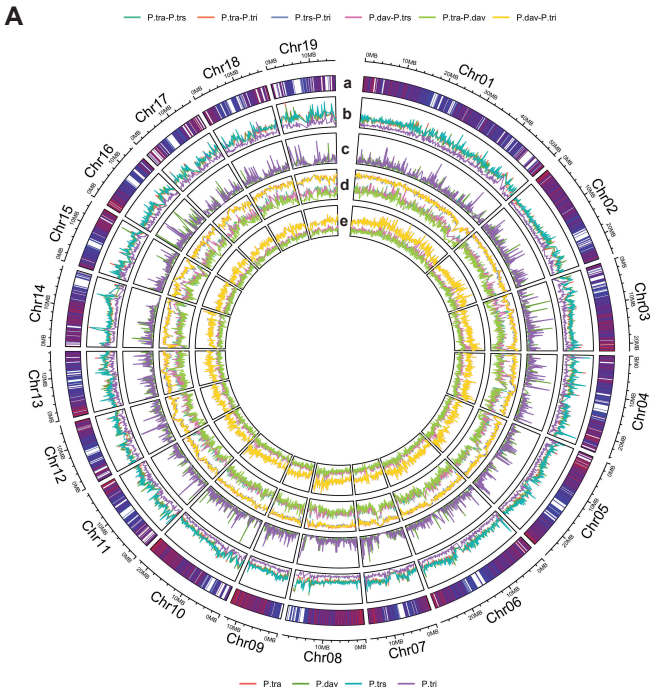
A
P.tra-P.trs
P.tra-P.tri
P.trs-P.tri
P.dav-P.trs
P.tra-P.dav
P.dav-P.tri
Chr01
Chr02
Chr03
Chr04
Chr05
Chr06
Chr07
Chr08
Chr09
Chr10
Chr11
Chr12
Chr13
Chr14
Chr15
Chr16
Chr17
Chr18
Chr19
a
b
c
d
e
P.tra
P.dav
P.trs
P.tri

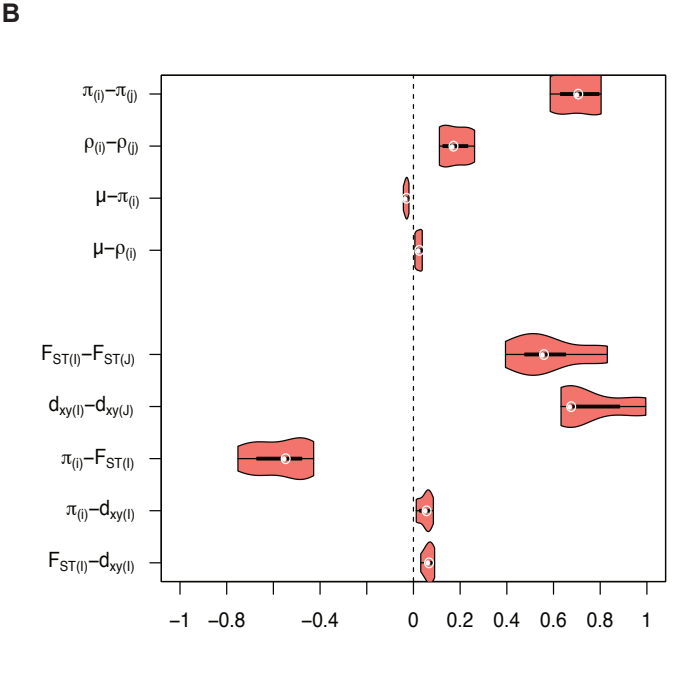
B
π(i)−π(j)
ρ(i)−ρ(j)
μ−π(i)
μ−ρ(i)
FST(I)−FST(J)
dxy(I)−dxy(J)
π(i)−FST(I)
π(i)−dxy(I)
FST(I)−dxy(I)
−1
−0.8
−0.4
0
0.2
0.4
0.6
0.8
1

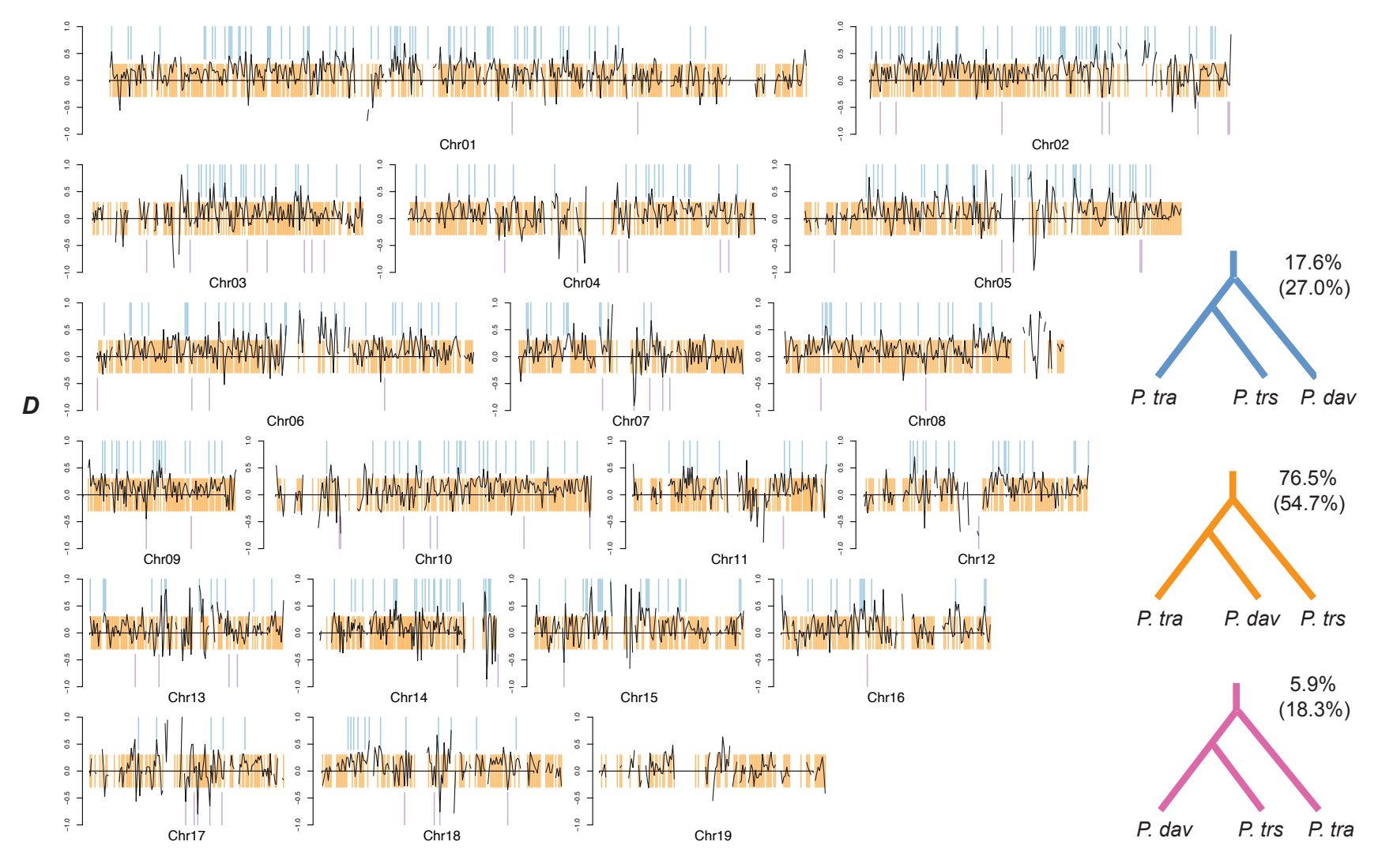
D
Chr01
Chr02
Chr03
Chr04
Chr05
Chr06
Chr07
Chr08
Chr09
Chr10
Chr11
Chr12
Chr13
Chr14
Chr15
Chr16
Chr17
Chr18
Chr19
17.6%
(27.0%)
P. tra
P. trs
P. dav
76.5%
(54.7%)
P. tra
P. dav
P. trs
5.9%
(18.3%)
P. dav
P. trs
P. tra

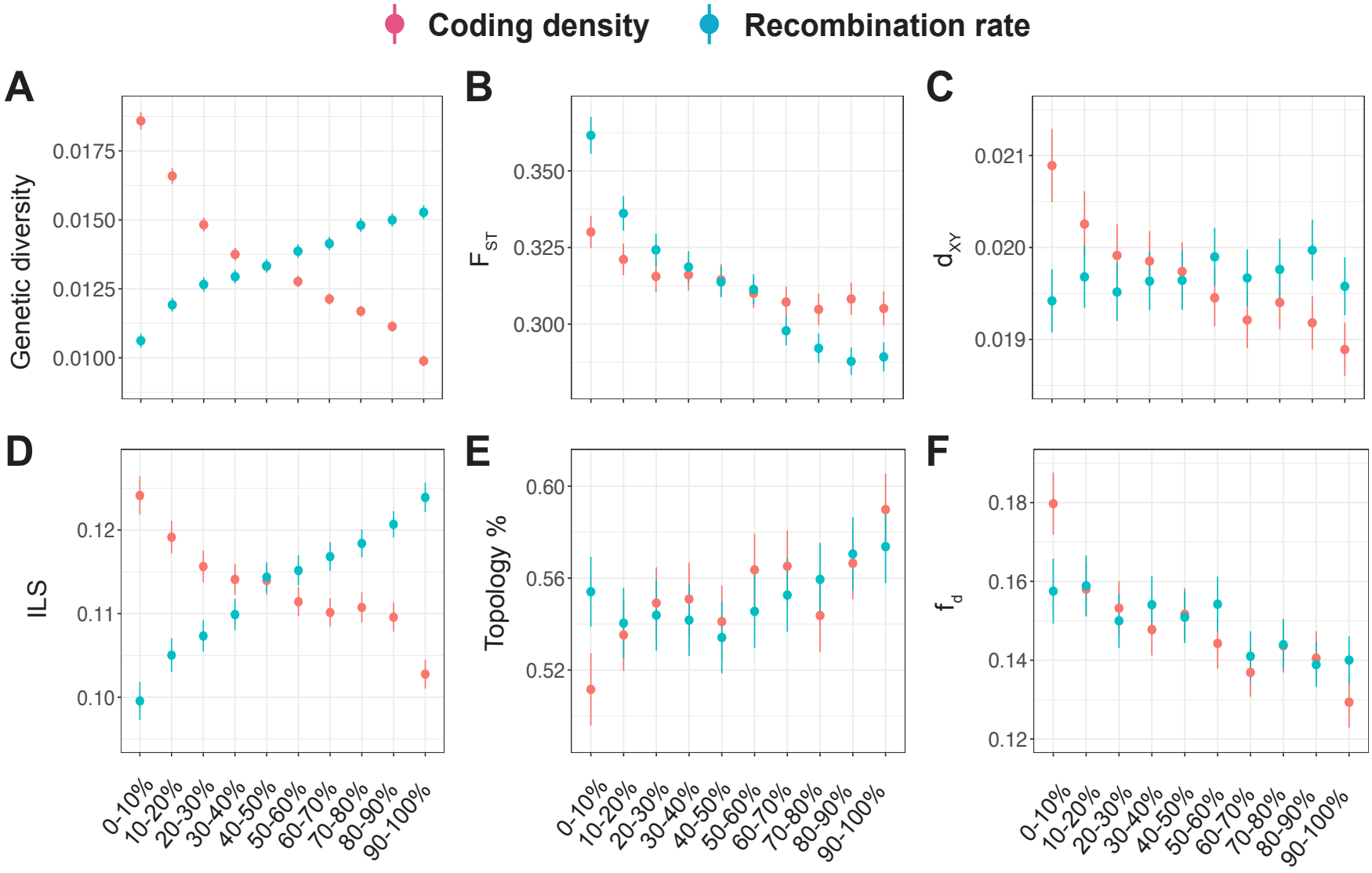
Coding density
Recombination rate
A
Genetic diversity
0.0175
0.0150
0.0125
0.0100
B
F_{ST}
0.350
0.325
0.300
C
d_{XY}
0.021
0.020
0.019
D
ILS
0.12
0.11
0.10
E
Topology %
0.60
0.56
0.52
F
f_d
0.18
0.16
0.14
0.12
0-10%
10-20%
20-30%
30-40%
40-50%
50-60%
60-70%
70-80%
80-90%
90-100%
Percentile of coding density and recombination rate

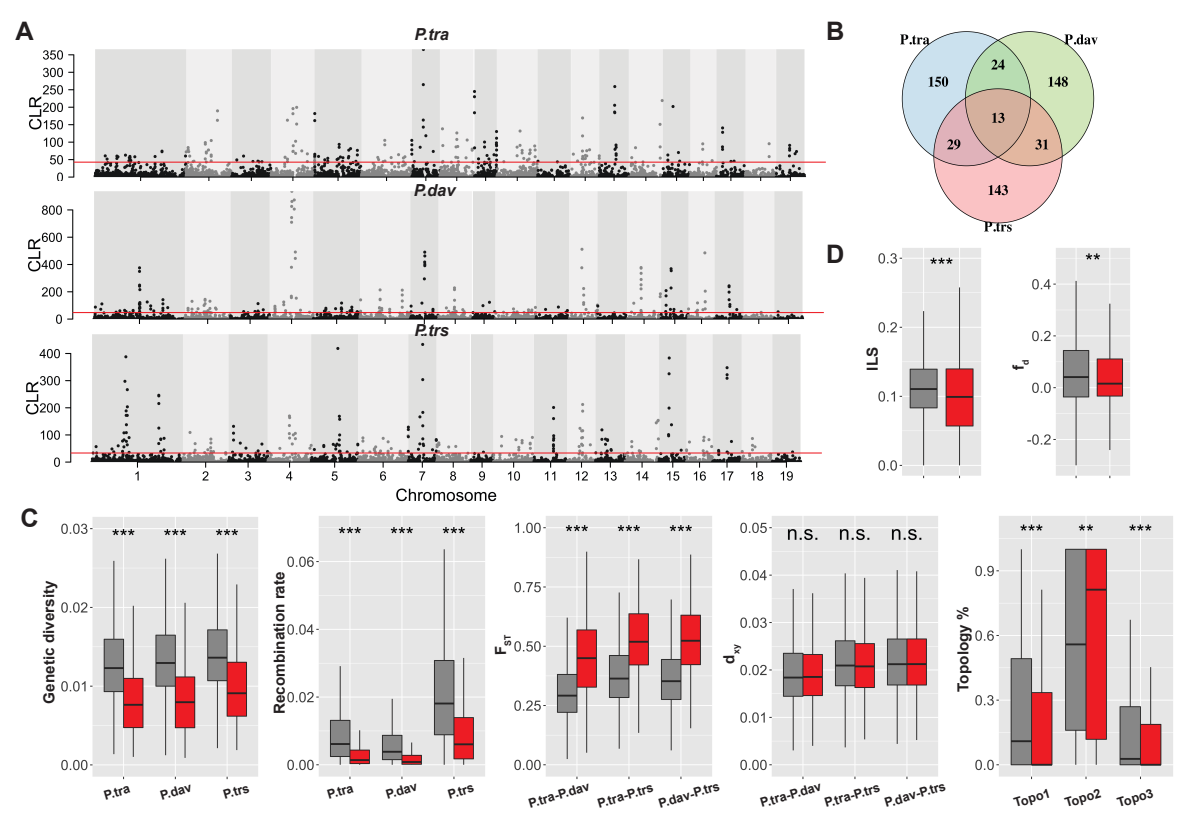
A
P.tra
P.dav
P.trs
CLR
Chromosome
B
P.tra
P.dav
P.trs
150
24
148
13
29
31
143
D
ILS
f_d
***
**
C
Genetic diversity
Recombination rate
F_{ST}
d_{xy}
Topology %
n.s.
P.tra
P.dav
P.trs
P.tra-P.dav
P.tra-P.trs
P.dav-P.trs
Topo1
Topo2
Topo3

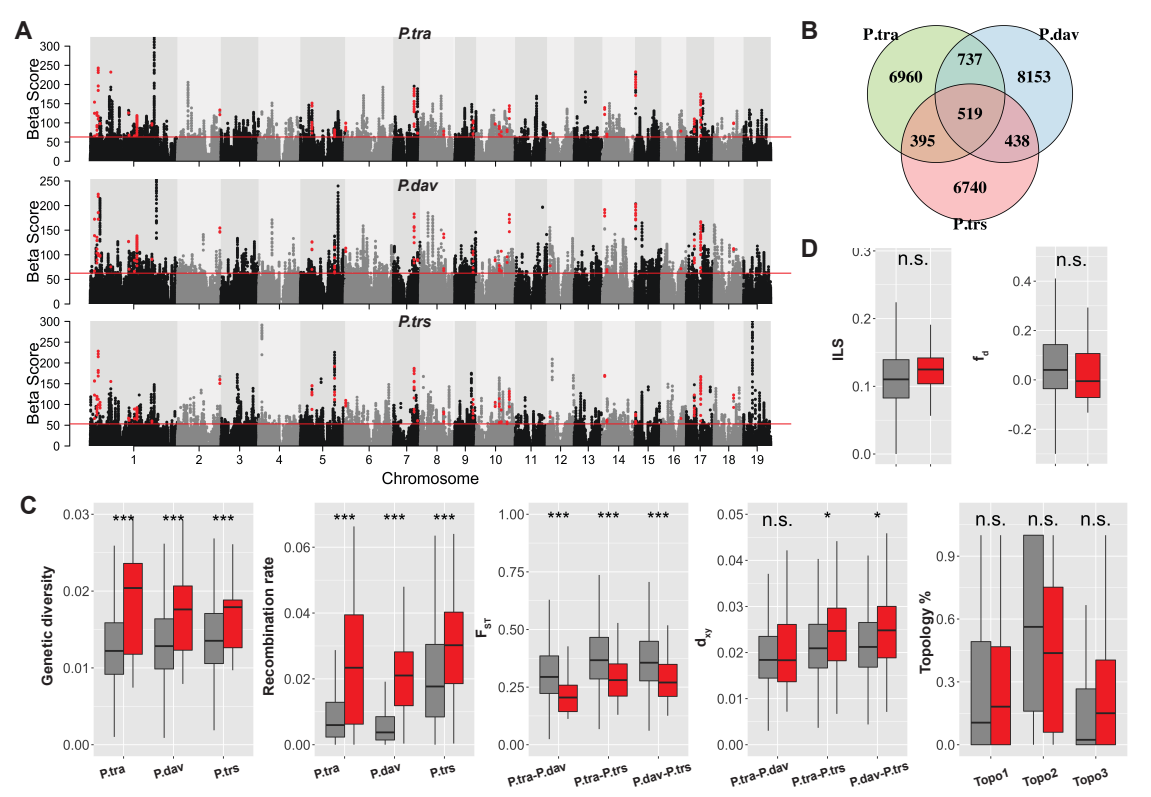
A
P.tra
P.dav
P.trs
Beta Score
Chromosome
B
P.tra
P.dav
P.trs
6960
737
8153
519
395
438
6740
C
Genetic diversity
Recombination rate
F_{ST}
d_{xy}
Topology %
P.tra
P.dav
P.trs
P.tra-P.dav
P.tra-P.trs
P.dav-P.trs
Topo1
Topo2
Topo3
***
*
n.s.
D
ILS
f_d
n.s.